


1-1-2011

Plesiosaur Body Shape and its Impact on Hydrodynamic Properties

Courtney D. Richards
richards84@marshall.edu

Follow this and additional works at: <http://mds.marshall.edu/etd>

 Part of the [Animal Sciences Commons](#), and the [Terrestrial and Aquatic Ecology Commons](#)

Recommended Citation

Richards, Courtney D., "Plesiosaur Body Shape and its Impact on Hydrodynamic Properties" (2011). *Theses, Dissertations and Capstones*. Paper 274.

This Thesis is brought to you for free and open access by Marshall Digital Scholar. It has been accepted for inclusion in Theses, Dissertations and Capstones by an authorized administrator of Marshall Digital Scholar. For more information, please contact zhangj@marshall.edu.

**PLESIOSAUR BODY SHAPE AND ITS IMPACT ON HYDRODYNAMIC
PROPERTIES**

A thesis submitted to
the Graduate College of
Marshall University

In partial fulfillment of
the requirements for the degree of Master of Science
in Biological Sciences

by
Courtney D. Richards

Approved by

Dr. F. Robin O'Keefe, Committee Chairperson
Dr. Brian L. Antonsen
Dr. Suzanne G. Strait

Marshall University
May 2011

Acknowledgments

I would like to extend my gratitude to my advisor, Dr. F. R. O'Keefe, and my committee members, Dr. B. Antonsen and Dr. S. Strait, for all of their guidance throughout this project. I am also grateful to Dr. D. Henderson for his work on the modeling portion of this study. Thanks to H. Zhu for her work on the *Tatenectes* reconstruction. I would also like to thank my fellow lab members, W. Holloway, B. Wilhelm, and N. Gardner. Thanks to the Natural History Museum, London, for allowing me access to their collections. This research was made possible by a MURC student travel grant.

This thesis would not have been possible without the encouragement and support that has been provided by all of my family and friends throughout the course of my graduate studies. I would particularly like to thank my parents, Wes and Jeanie; my siblings, Nathaniel, Chelsea, and Seth; and my good friends, John and Kate.

Table of Contents

Acknowledgments	ii
List of Figures and Tables	v
Abstract	vii
Chapter 1-Introduction	1
Background on Plesiosauria	1
Study Taxa	3
Hydrostatic Buoyancy	6
Modeling Extinct Taxa	11
Research Objective	19
Chapter 2-Plesiosaur Reconstructions	21
Introduction	21
Materials and Methods	21
Materials	21
Photographs	22
Vertebrae and Girdle Articulation	23
Centrum Angles	24
Rib Orientation	27
Transverse Cross Section	28
Results	29
Discussion	44
Chapter 3-Plesiosaur Buoyancy and Stability	46
Introduction	46

Materials and Methods.....	47
Materials	47
Methods.....	47
Tests	52
Results.....	54
Models.....	54
Tests	55
Discussion.....	60
Comparison.....	60
Habitat Implications.....	63
Possible Sources of Error.....	64
Future Work	64
Conclusion	65
Literature Cited	66

List of Figures and Tables

Figure 1.1. Pliosauromorph and plesiosauromorph body shapes	2
Figure 1.2. Plesiosaur phylogeny.....	4
Figure 1.3. Cryptocleidoidea relationships	6
Figure 1.4. Pachyostosis in <i>Tatenectes</i>	7
Figure 1.5. Body shape approximation.....	12
Figure 1.6. <i>Tyrannosaurus rex</i> outline.....	14
Figure 1.7. <i>Tyrannosaurus rex</i> 3-D mesh.....	16
Figure 2.1. <i>Cryptoclidus</i> rib orientation.....	28
Figure 2.2. <i>Tatenectes</i> reconstruction	32
Figure 2.3. <i>Cryptoclidus</i> reconstruction.....	33
Figure 2.4. <i>Muraenosaurus</i> reconstruction.....	34
Figure 2.5. Transverse cross-sections	35
Table 2.1. <i>Tatenectes</i> centra angle.....	36
Table 2.2. <i>Cryptoclidus</i> centra angles.....	37
Table 2.3. <i>Muraenosaurus</i> centra angles	39
Table 2.4. <i>Tatenectes</i> wedging angles	39
Table 2.5. <i>Tatenectes</i> anteroposterior wedging angles.....	40
Table 2.6. <i>Cryptoclidus</i> wedging angles.....	41
Table 2.7. <i>Cryptoclidus</i> anteroposterior wedging angles.....	42
Table 2.8. <i>Muraenosaurus</i> wedging angles	43
Table 2.9. <i>Muraenosaurus</i> anteroposterior wedging angles.....	44
Figure 3.1. 3D slicing method.....	48

Figure 3.2. Lung position.....	50
Figure 3.3. Models at equilibrium.....	57
Figure 3.4. Buoyant recovery.....	58
Table 3.1. The effects of lung deflation on body mean density and buoyancy	59
Figure 3.5. Lateral roll recovery	61

Abstract

Plesiosaur body shape and its impact on hydrodynamic properties

By Courtney D. Richards

Despite the variability of cross-sectional body shape within Plesiosauria, its impact on plesiosaur buoyancy and stability has never been investigated. This study focused on *Tatenectes*, *Cryptoclidus*, and *Muraenosaurus* due to their variable body morphologies. Reconstructions were created based on measurements and photographs from fossil remains. The ability of computer models, based upon the reconstructions, to reach equilibrium after submersion, sink via lung deflation, and recover from a lateral roll was tested. For the computer models, *Muraenosaurus* was replaced with *Thalassomedon*, which had a similar morphology. *Cryptoclidus* and *Thalassomedon* recovered from submersion faster than *Tatenectes*. All models achieved negative buoyancy with 85-95% lung deflation. *Tatenectes* and *Cryptoclidus* recovered from lateral roll quickly, 10 and 12 cycles respectively, compared to *Thalassomedon* (25 cycles). The findings suggest that dorsoventrally compressed plesiosaurs, such as *Tatenectes* and *Cryptoclidus*, inhabited shallow-waters and deep-bodied genera, such as *Thalassomedon* and *Muraenosaurus*, inhabited deep-water environments.

Chapter 1. Introduction

BACKGROUND ON PLESIOSAURIA

The Plesiosauria was a clade of secondarily aquatic marine reptiles (O’Keefe, 2002; Henderson, 2006; Druckenmiller and Russell, 2008), meaning that the ancestors of plesiosaurs were terrestrial and plesiosaurs secondarily returned to the water. Plesiosaurs first evolved in the Rhaetian stage of the Upper Triassic epoch about 200 million years ago (Storrs and Taylor, 1996), and went extinct in the Maastrichtian stage of the Upper Cretaceous about 65 million years ago during the end-Cretaceous mass extinction event (O’Keefe, 2002; Henderson, 2006) that wiped out about 76 percent of all species (Kriwet and Benton, 2004), including the non-avian dinosaurs. The first plesiosaurs were scientifically described in the early 1820s from fossils found by the fossil collector Mary Anning, in the Lyme Regis region of England (Conybeare, 1824; Tarlo, 1960).

Plesiosaurs are now known to have a worldwide fossil distribution (Gasparini et al., 2003; O’Keefe and Carrano, 2005; Druckenmiller and Russell, 2008; Ketchum and Benson, 2010).

Plesiosaurs ranged in size from about 2 meters to 14 meters in length (Brown, 1981). They are highly specialized for their aquatic environment. The gastralia basket and massive pectoral and pelvic girdles form a ridged trunk in plesiosaurs (Lin and Rieppel, 1998; O’Keefe and Carrano, 2005). The forelimbs and hind limbs are both well developed hydrofoils capable of providing paraxial propulsion instead of relying on lateral undulation as in primitive sauropterygians (Lin and Rieppel, 1998).

There are two basic plesiosaur body types, plesiosauromorphs and pliosauromorphs (Fig.1.1). Plesiosauromorphs are plesiosaurs that possessed long necks

consisting of at least 28 cervical vertebrae, relatively small heads, and humeri that are larger than the femura. Pliosauromorphs are plesiosaurs that had short necks made up of 13 to 28 cervical vertebrae, relatively large heads, and femura that are larger than the humeri (Brown, 1981; O'Keefe, 2002; O'Keefe and Carrano, 2005). Historically, these two morphotypes have been interpreted as representing two separate superfamilies of plesiosaurs (Plesiosauroidea and Pliosauroidae) (Brown, 1981). Recent cladistic analyses of the Plesiosauria show that the pliosaur body shape evolved independently multiple times with at least one evolution taking place in the Plesiosauroidea. However, plesiosaur relationships are a very complex and heavily debated topic (Carpenter, 1996; O'Keefe, 2001, 2002; Druckenmiller and Russell, 2008; Smith and Dyke 2008; Ketchum and Benson, 2010).

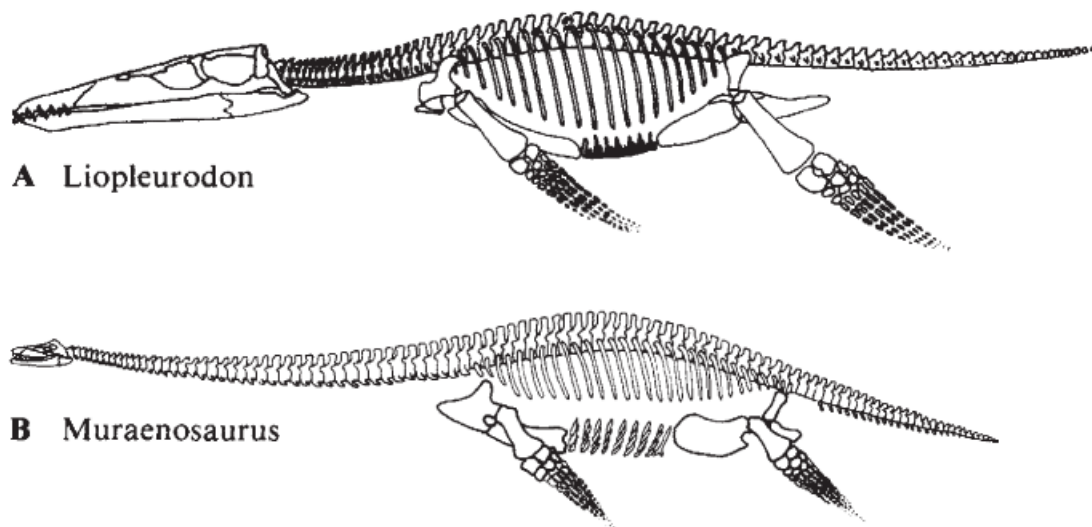


Figure 1.1. Pliosauromorph and plesiosauroidean body shapes. A. *Liopleurodon*, an example of the short necked, large skulled pliosauromorph body shape. B. *Muraenosaurus*, an example of the long necked, small skulled plesiosauroidean body shape. Figure from Taylor (1981).

The most recent cladistic analysis of plesiosaurs, done by Ketchum and Benson (2010) (Fig 1.2), found Rhomaleosauridae to be monophyletic. This finding is in accordance with O’Keefe et al. (2001) and Smith and Dyke (2008). For the first time in a cladistic analysis, Leptocleididae formed a sister group to Polycotylidae and both fell within Plesiosauroidea. This finding supports the hypothesis that plesiosauroid and pliosauroid body shapes do not form two separate taxonomic groupings, but rather evolved multiple times within both Plesiosauroidea and Pliosauroidea. Also for the first time, Plesiosauridae was found to be a monophyletic group (Ketchum and Benson, 2010). However, as noted by Ketchum and Benson (2010), homoplasy is common within plesiosaur phylogenies, suggesting that more work still needs to be done to better resolve the clade.

STUDY TAXA

Of particular interest to the study discussed in Chapters 2 and 3, are three cryptocleidoids, *Cryptoclidus eurymerus*, *Muraenosaurus leedsii*, and *Tatenectes laramiensis*. These three genera cover the currently known range of cross-sectional body shapes ranging from dorsoventrally compressed in *Tatenectes* to laterally compressed in *Muraenosaurus* with *Cryptoclidus* possessing an intermediate cross-sectional shape (O’Keefe et al., 2011). *Cryptoclidus* and *Muraenosaurus* are both known from the Upper Jurassic (Callovian) Oxford Clay Formation of southeast England (Brown, 1981). The Oxford Clay Formation is interpreted as being deposited in a shallow, epicontinental sea with depths ranging from 10-50 meters (Cruickshank et al., 1996). *Tatenectes laramiensis* is a North American cryptocleidoid from the Upper Jurassic (Oxfordian) Sundance Formation of Wyoming. *Tatenectes* is known from the top of the formation, which was

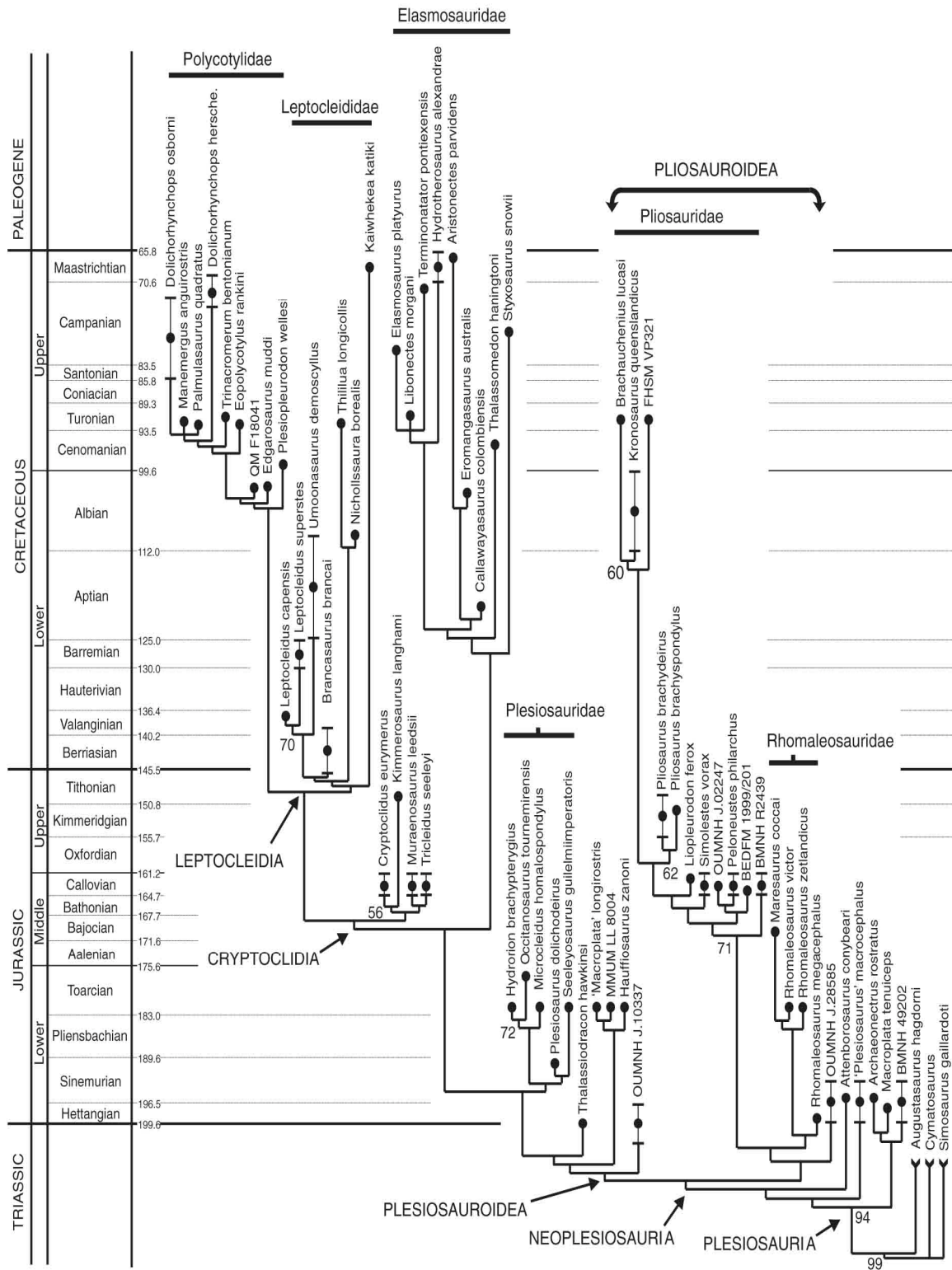


Figure 1.2. Plesiosaur phylogeny. Ketchum and Benson (2010) phylogenetic analysis including 66 taxa scored on 178 characters. Figure from Ketchum and Benson (2010).

deposited in a nearshore environment of a shallow epicontinental seaway (O'Keefe and Street, 2009).

Cryptoclidus eurymerus is a moderately sized plesiosaur with adult individuals reaching an average length of four meters. There are a total of 55 presacral vertebrae: 32 cervical vertebrae, three pectoral, and 20 dorsal. There is some variation in the location of the pectoral vertebrae along the vertebral column. This pectoral vertebrae migration results in varying numbers of cervical and dorsal vertebrae within the genus, however, the number of total presacral vertebrae remains consistent. The interclavicle is reduced to a rarely preserved splint of bone (Brown, 1981).

Muraenosaurus leedsii was originally thought to be an elasmosaurid on the basis of its highly elongated neck, however, recent analysis have placed it within the Cryptocleidoidea (Fig. 1.3) (O'Keefe, 2001, 2002; O'Keefe and Street, 2009).

Muraenosaurus has 66 presacral vertebrae: 44 platycoelous cervical vertebrae, three pectoral, and 19 dorsal. As with *Cryptoclidus*, the location of the pectoral vertebrae is variable, resulting in slight deviations from this vertebral formula. Longitudinal crests on the anterior cervical vertebrae provided muscle attachment points that were likely necessary for support. Adult individuals are larger than *Cryptoclidus*, reaching lengths of about 5.2 meters. The dorsal vertebrae in *Muraenosaurus* are proportionally longer than in *Cryptoclidus*, while the opposite relationship is true in the caudal vertebrae. The interclavicle is a well developed bone in *Muraenosaurus* (Brown, 1981).

Tatenectes laramiensis was a small plesiosaur, only about two meters long. The number of cervical vertebrae is unknown due to the incomplete nature of the specimens. The cervical vertebrae that are preserved are anteroposteriorly compressed compared to

the conditions of *Cryptoclidus* and *Muraenosaurus*. There is possible preservation of an interclavicle, but it may be a clavicle instead (O’Keefe and Street, 2009). The gastralia in *Tatenectes* are pachyostotic, which not only differs from the gastralia of *Cryptoclidus* and *Muraenosaurus*, but from all other known plesiosauiromorphs as well (Street and O’Keefe, 2010).

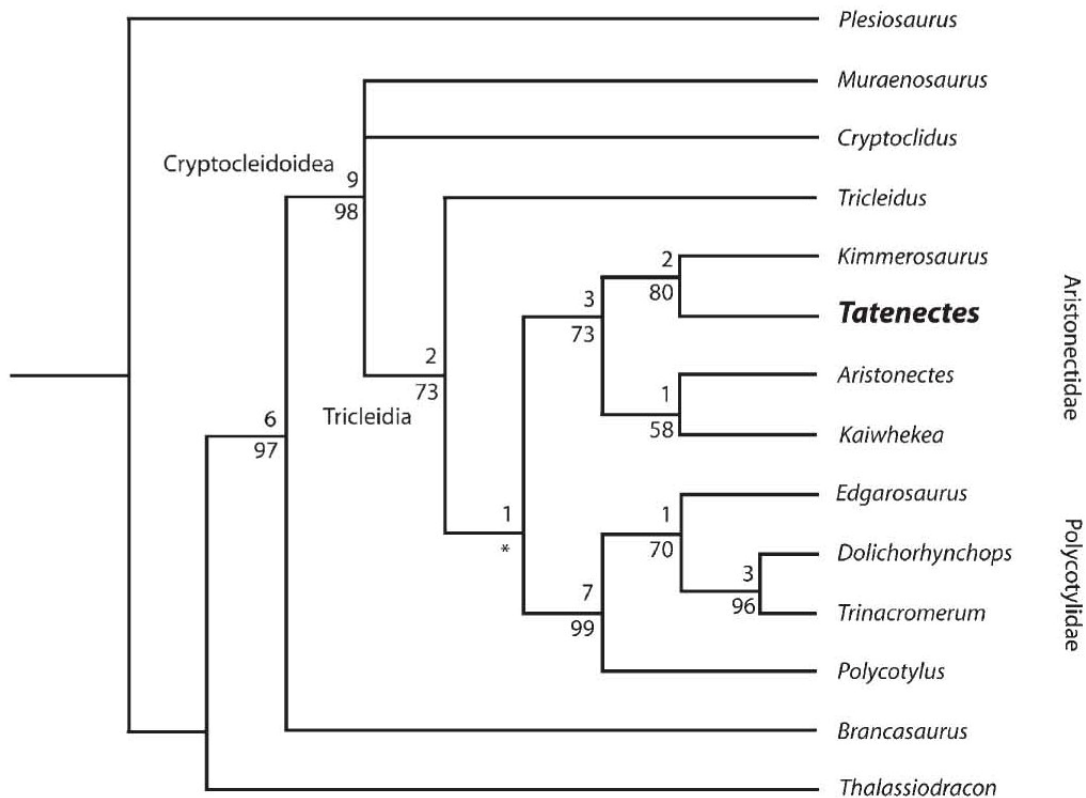


Figure 1.3. Cryptocleidoidea relationships. A phylogenetic analysis of 11 Cryptocleidoidea taxa with three outgroup taxa. The character matrix included 90 cranial and postcranial morphologies. Figure from O’Keefe and Street (2009).

HYDROSTATIC BUOYANCY

Hydrostatic buoyancy is the upward force exerted on an object that is floating in still water. An object that is floating at the surface is said to be positively buoyant, whereas an object that sinks is negatively buoyant (Lautrup, 2005). Aquatic animals need

to be able to control their buoyancy in order to be able to both float at the water's surface and initiate and maintain underwater dives (Henderson, 2003). There are several different methods of buoyancy control that have been proposed for plesiosaurs and other marine taxa.

Pachyostosis—Pachyostotic is a term used to describe relatively thickened and dense bone (Fig. 1.4) (Cruickshank et al., 1996; Street and O'Keefe, 2010). This condition differs from the normal trend seen in marine animals, where bone mineralization is reduced in order to increase buoyancy and maneuverability. Although a common condition in some secondarily aquatic animals, such as sirenians, cases of pachyostosis within Plesiosauria are rare. Instances have been reported for the pliosaurs *Kronosaurus boyacensis* and *Pachycostasurus dawni* (Cruickshank et al., 1996), and in the gastralia of the plesiosaur *Tatenectes laramiensis* (Street and O'Keefe, 2010). It

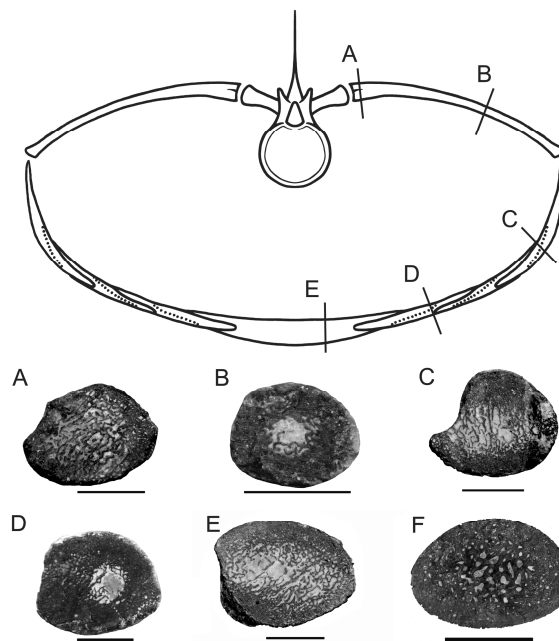


Figure 1.4. Pachyostosis in *Tatenectes*. A-E are cross-sections through some of *Tatenectes* pachyostotic bones. F is a cross-section through non-pachyostotic, *Pantosaurus* bone. Figure from Street and O'Keefe (2009).

should be noted that the pachyostosis exhibited in *Tatenectes* is odd in that the bone is actually a combination of pachyostotic and osteoporotic bone. So, while the diameter of the bone is increased, the overall density of the bone may not differ from those of taxa that display neither condition (Street and O’Keefe, 2010).

The pachyostotic bone is thought to act as ballast and increases the volume, surface area, and cross sectional area of the bone. The increased, ventral mass would provide negative buoyancy to help cancel out some of the positive buoyancy provided by the lungs (Cruickshank et al., 1996). A side effect of increasing bone density is a decrease in maneuverability and speed. These functional considerations, along with the ecology of extant *Serenia* has led to the interpretation of pachyostotic animals as inhabiting shallow marine environments where stability is favored over maneuverability (Street and O’Keefe, 2010).

Gastroliths—The function of gastroliths (stomach stones) found associated with plesiosaur fossils has been a source of contention since their early discovery (Brown, 1904). There are two major hypotheses that have been proposed. The first is that gastroliths were swallowed to aid in the breakdown and mixing of food material, as is seen in extant birds. Plesiosaurs are sometimes thought of as having a diet comprised solely of fish, however, preserved gut contents reveal that many also fed on shelled invertebrates (Brown, 1904; McHenry et al., 2005). The remains of the shelled invertebrates within the stomach cavity are crushed. Plesiosaur teeth are not functional for crushing hard material; however, the stomach cavity also contained gastroliths. These gastroliths would have been capable of the gastric milling of shelled material (Brown, 1904; McHenry et al., 2005).

The second hypothesis is that gastroliths were swallowed for ballast (Wing, 2007), as has been suggested for a variety of extant semi-aquatic animals, including crocodiles (Taylor, 1981), penguins (Beaune et al., 2009), seals, and sea lions (Wing, 2007). Taylor (1981) proposed that the lungs in plesiosaurs would have made them too buoyant to dive. As it is fairly well accepted that plesiosaurs must have done at least some diving, he suggested that gastroliths were used by plesiosaurs as ballast. The reasoning behind this idea was that modern crocodiles have been shown to use stones to help them stay underwater with only their eyes exposed as they wait for prey. There have been several plesiosaur fossils found with gastroliths in the stomach region that also contain the remains of prey that were not pulverized, which suggests that Plesiosaurs were using gastroliths for something other than grinding food (Taylor, 1981). As Taylor conducted a purely qualitative study, the theory of gastroliths as plesiosaur ballast was untested.

In 2006, Henderson approached the same question as Taylor with a computer modeling study, using methods discussed in the next section. He used varying amounts of gastroliths and placed them in the area of the model plesiosaur's trunk region where the stomach probably would have been located in life based on stomach location in extant reptiles. He tested the effect of gastroliths on negative buoyancy. It was determined that the amount of gastroliths needed to make an impact on plesiosaur buoyancy was a mass greater than 10% of the animal's total body mass, which is not plausible, and far exceeds the number of gastroliths that have ever been found associated with plesiosaur fossils (Henderson, 2006).

Before conducting his study of the effect of gastroliths on plesiosaur buoyancy, Henderson used a similar method of 3-D modeling to quantitatively test the effect of

stomach stones in crocodiles. It was shown that a mass of stones more than 6% of the crocodile's total body mass was needed for the model to exhibit negative buoyancy. This value exceeds the reported mass of gastroliths actually found in crocodiles, which is less than 2% of the total body mass (Henderson, 2003). Findings similar to Henderson's (2003, 2006) have been reported for a variety of extant animals. As mentioned earlier, penguin species have been shown to ingest gastroliths. A computational study on the function of gastroliths in king penguin chicks showed that it is unlikely that the gastroliths were used for ballast. The reasoning for this conclusion was the same as the computational studies in plesiosaurs; the mass of the gastroliths was too small compared to the mass of the animal to have a substantial impact on buoyancy (Beaune et al., 2009). Therefore, it is likely that gastroliths were utilized for gastric milling rather than buoyancy control (Brown, 1904; McHenry et al., 2005).

Lungs Inflation and Deflation—After the effects of pachyostosis and gastroliths on buoyancy control were tested and found to have a negligible impact, researchers looked at the effect of inflation and deflation of the lungs on buoyancy. Henderson (2003, 2006), Beaune et al. (2009), and Wing (2007) all came to conclusion that deflation of the lungs is the method that is most likely utilized for ballast. In whales, a decrease in lung volume due to pressure changes is theorized to help them maintain negative buoyancy (Nowacek et al., 2001). It was found that crocodiles became negatively buoyant after deflation of the lungs by around 50% (Henderson, 2003) and the plesiosaurs that were modeled (*Cryptoclidus*, *Liopleurodon*, and *Thalassomedon*) were negatively buoyant between 85% and 90% lung deflation. This means that plesiosaurs would have been able to initiate a dive by just adjusting the volume of their lungs (Henderson, 2006).

MODELING EXTINCT TAXA

Using models to estimate parameters about extinct taxa is not a new concept. It has been in use since the early 1900s. It was first done in 1905 when a study was conducted by Gregory to determine the weight of an *Apatosaurus*. To accomplish this, a scaled model of an *Apatosaurus* was constructed taking into account the possible musculature. The experiment used the principle that the volume of an object is equal to the volume of water it displaces. After the amount of water displaced was calculated, the weight of the water was measured and multiplied by the scale of the model in order to obtain an estimate of the weight of a living *Apatosaurus*. It was noted that the weight was probably greater than the calculated estimate of 34 ¼ tons, so an extra 10% was added for a final weight estimate of 38 tons (Gregory, 1905). There were several places for error to occur as was pointed out by later researchers. One source of error was the addition of the extra 10% to the final weight. Another source of error was not taking specific gravity, the ratio of the density of the model to the density of water, into account (Colbert, 1962). In 1962, Colbert expanded on the 1905 study conducted by Gregory. Colbert used the same basic methods as described by Gregory, with the only real difference being that sand was utilized instead of water and unlike Gregory, Colbert realized the importance of taking specific gravity into account when estimating weight (Colbert, 1962).

Neither Colbert nor Gregory took into account how the mass was distributed within the animals, which limits the usefulness of the studies. Another possible flaw in the estimates is that even a small error in the dimensions of the scaled models can result in large errors in the calculated weights due to the exaggeration of the errors through multiplication when converting from a one dimensional value to volume and converting

from scaled model size to actual size. More advanced modeling methods are necessary in order to obtain the information about mass distribution and to help cut down on erroneous estimates due to scaled model imperfections (Henderson, 1999).

In 1988, Massare took the idea of simple models a step further, conducting a study to estimate the maximum sustained swimming speeds of plesiosaurs as well as some other genera of marine animals (Massare, 1988). An animal's body shape, surface area, volume, and mode of propulsion all play an important role in their swimming speed (Massare, 1988; Motani, 2002), so estimates needed to be made. Massare drew from previous studies to gather information about the methods of propulsion of the various animals used in her study. For plesiosaur locomotion, Massare used the currently accepted theory that a combination of underwater flight and rowing fin motions were used for propulsion. Massare calculated the surface area and volume by using a prolate spheroid (elongated spheroid) to approximate the body shape (Fig. 1.5). Using the estimated values of surface area and volume, set values for muscular efficiency and metabolic rate, and estimated values of propulsive efficiency (based on the method of propulsion), sustained swimming speeds were calculated (Massare, 1988).

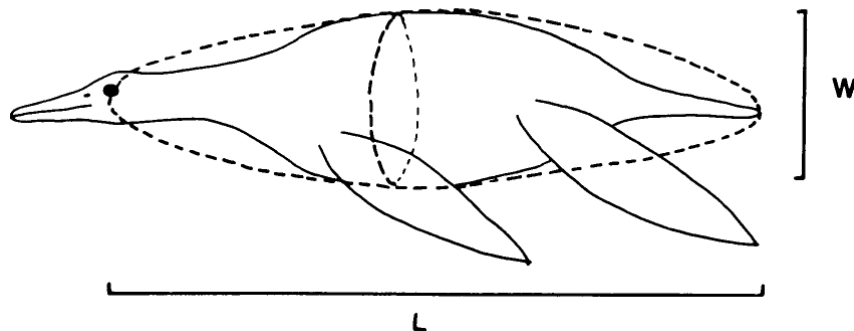


Figure 1.5. Body shape approximation. A plesiosauromorph shown with the prolate spheroid used to approximate its body shape. The length of the animal is the major axis, the depth or width is the minor axis (the diameter of the circular cross-section of the prolate spheroid). Figure from Massare (1988).

In her 1988 paper, Massare pointed out several flaws with her modeling method and cautioned that it was only precise enough to determine differences between animals with very different body shapes; it was not precise enough to accurately determine differences at the species or individual level. Some of the flaws that Massare noted were the assumption that all marine reptiles can be approximated by a single geometric shape, and the assumption of a set value for the metabolic rate of all marine reptiles (Massare, 1988).

In 2002, Motani revisited this question of plesiosaur swimming speed using a more advanced modeling method. Motani stated that revising swimming speeds was necessary because of the sources of error that Massare pointed out in her study, and because of calculation errors that Motani discovered. Motani used similar calculations as Massare, but was able to improve on her method by using computer modeling (discussed in a later section). Motani was able to more accurately represent the various body shapes by approximating them with a series of superellipses instead of a single geometric shape. With a better model of body shape, the calculations of volume and surface area become more accurate. With updated information on the metabolic rates of reptiles, improved estimates of volume and surface area, and corrected equations, Motani was able to obtain estimates of optimal speed. While Motani's results differ from Massare's, they propose the same relative swimming speeds, with the pliosauromorphs and plesiosauromorphs having similar estimated speeds (0.51 and 0.49 m/sec respectively) that were less than the estimated speeds for marine animals such as fish (1.2 m/sec), seals (1.0 to 1.5 m/sec), dolphins (2.5 m/sec), and whales (3 m/sec) (Motani, 2002).

Computer Models—In 1999, Henderson developed a new method of modeling extinct taxa. It is a mathematical method that calculates the volume, mass, and the position of the center of mass, all of which are essential variables in gaining an understanding of how an animal moves. The first step is to collect the animal's outline from scientific drawings of the animal in side and top view, including the known (in the case of extant taxa) or probable (in the case of extinct taxa) skeletal structure, musculature, and skin. The outlines are plotted as graphed points with the longitudinal dimension as the x-axis, the vertical dimension as the y-axis, and the horizontal dimension as the z-axis (Fig. 1.6). These plots are done by using a digitizing stylus and a computer-aided drafting program (CAD) (Henderson, 1999).

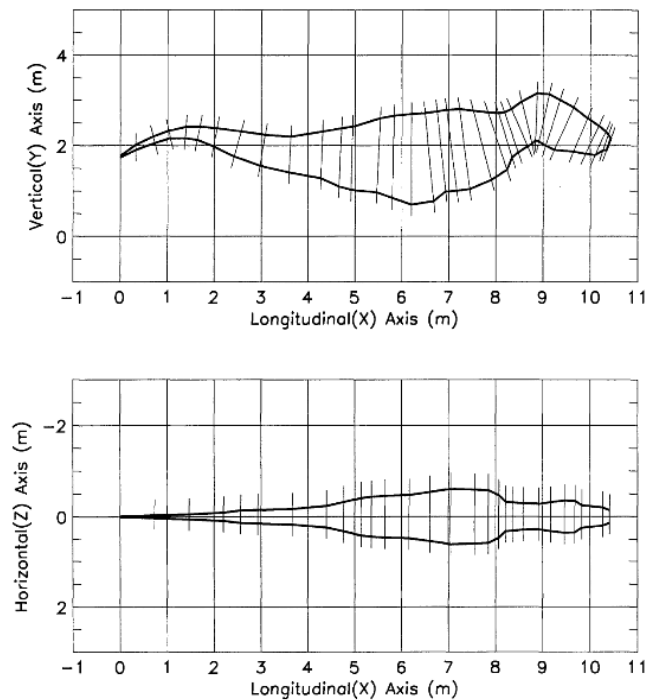


Figure 1.6. *Tyrannosaurus rex* outline. Outline of a *T. rex* in side and top view plotted on the xy and xz planes with lines drawn to break the outline into segments. Figure from Henderson (1999).

The outlines are broken into numerous segments with curved areas, such as the neck, being represented by more segments than flatter regions, such as the thoracic region. The xy and xz intercepts of the segment lines with the animal's outline are used to define the radii of a series of ellipses that form a 3-D mesh made up of polygons (Fig. 1.7). The ellipses are subdivided further into subslabs and the volume of each subslab is computed using methods described in depth in Chapter 3. To obtain the volume of the entire animal, the volumes of all of the subslabs are summed and the mass can then be determined by multiplying the volume by an assumed density. For his 1999 study, Henderson used a uniform tissue density of 1000 kg/m^3 for all of the animals, both extinct and extant, which Henderson admits could be a source of error for some of his models. In the case of marine animals in Henderson's 2006 study, the assumed animal density was set to 1050 kg/m^3 (Henderson, 2006). Once the mass is estimated, further computer calculations can determine the center of mass in three-dimensional space. The more slabs into which the outline is divided, the more accurate the estimates of volume, mass, and center of mass become (Henderson, 1999). An even more accurate center of mass estimate can be obtained if the model takes into account the volume and position of lungs. For extinct reptiles, Henderson used a lung volume estimate of 10% of the total body volume and placed the lungs in the anterior region of the chest based on lung data from a variety of extant reptiles including leatherback turtles and alligators (Henderson, 2006).

As with scaled physical models, there are several possible sources of error with Henderson's method that could lead to erroneous estimates. If the outlines of the body, from which all of the calculated estimates are made, are incorrect, it can result in a

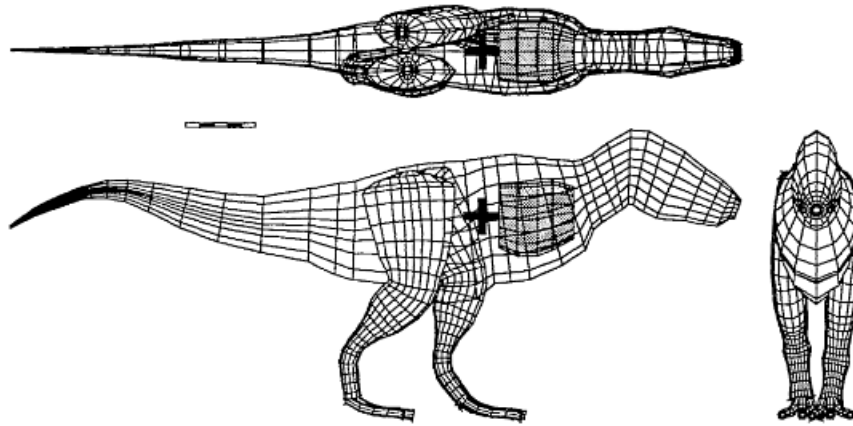


Figure 1.7. *Tyrannosaurus rex* 3-D mesh. Top, side, and front views of a *T. rex* 3-D mesh, where “+” represents the center of mass and the slightly darker region seen in the chest region of the top and side views represent the lungs. Figure from Henderson (1999).

dislocation of the center of mass. Another source of error can occur when the x-axis, y-axis, and z-axis (representing the length, width, and height, respectively) are plotted because the points are manually collected using a digitizing stylus. Finally, incorrect reconstructions (on which the outlines are based) that either overestimate or underestimate the mass in a particular region of the animal’s body will lead to overall errors in both mass and the center of mass (Henderson, 1999).

In addition to reiterating the flaws in Henderson’s model that he acknowledged in his 1999 paper, a study by Motani (2001) investigated a few other possible problems with using ellipses to estimate body shape. Motani’s study of the body shape of extant animals determined that their body cross sections were not, in fact, elliptical and, therefore, ellipses should not be used to model extinct taxa, as it stands to reason that they would not have perfectly elliptical cross sections either. With this in mind, Motani developed a computer modeling method that is similar to Henderson’s 1999 method, except that

Motani uses superellipses instead of ellipses to approximate body shape because they allow for greater variability in cross-sectional shape. Also, instead of calculating mass and center of mass, Motani's model calculates mass and surface area (although Motani does note that his model could be modified in the future to include center of mass calculations) and does not take into account the presence lungs (Motani, 2001). Both models included variables that were geared toward the specific questions that the researchers wanted to address. Later works by Henderson (2003, 2006) focused on buoyancy in plesiosaurs, where adding the lungs to the model is essential. However, Motani's later research (2002) was more geared toward estimating swimming speeds, on which the inclusion of lungs in the model is not expected to have much of an impact.

While the cross-sectional shapes of Motani's models were shown to be more accurate representations of what is found in nature than Henderson's models, the same sorts of problems with the method exist. Although it is true that not all body shapes seen in nature are accurately approximated by ellipses, it is also true that not all body shapes can be approximated by superellipses. As with Henderson's method, errors in Motani's model occur when there are errors in the assumed cross section of the animal that is being studied. If there are not accurate cross sections based on measurements from the fossil evidence, then the approximation of the cross sections using either ellipses or superellipses will not represent reality. Not only will all of the calculations based on the approximations will be skewed, but errors already present within the modeling process will be compounded (Motani, 2001). So, with either modeling method, the first step is to obtain the most accurate reconstruction of the study animal that is available.

Another method of modeling that has only recently been developed is the ATD method. The measurements required are the anteroposterior length, transverse width, and dorsoventral depth. After the measurements are obtained, linear regression analyses can be used to predict the volume. While the ATD method is much simpler to perform than the more calculation-heavy methods of Henderson (1999) and Motani (2001) the ATD method has only been used to make estimates of volume instead of mass (Novack-Gottshall, 2008). Without knowing the distribution of body mass, questions about functional morphology of an animal will be limited, since understanding mass distribution is essential to understanding how an animal balances and moves (Henderson, 1999).

Testing the Accuracy of Models—In order to test whether a model is giving reliable approximations for mass, or volume, the models must be used to run calculations for simple objects or for extant animals with known mass and volumes (Massare, 1988; Motani, 2002; Novack-Gottshall, 2008). If the models are able to accurately determine the values for simple shapes, then extant animals are modeled to test how accurately the models predict their mass or volume. The calculated values for extant animals from the models are compared to values published in the scientific literature. Some discrepancy between calculated estimates from the models and values cited in the literature is to be expected as the literature often only contains measurements from a few individuals for any given species and will not necessarily take into account variation in size and shape within that given species (Massare, 1988; Henderson, 1999; Motani, 2001, 2002; Novack-Gottshall, 2008). In the case of marine reptile models, aquatic animals such as whales, dolphins, crocodiles, and sea turtles are often used for comparison (Massare,

1988; Henderson, 1999; Motani, 2001) as they are the extant animals that are believed to have the most similar lifestyles and tissue densities to plesiosaurs. The more accurately a model estimates the simple shapes and extant taxa, the more confident the researchers can be that the model is producing accurate predictions for the extinct taxa being studied (Massare, 1988; Henderson, 1999; Motani, 2001, 2002; Novack-Gottshall, 2008).

The method developed by Henderson (1999, 2003, 2006) will be used to estimate the hydrodynamic properties in plesiosaurs in Chapter 3. Henderson tested the accuracy of this method in 2003 using alligators as his study animal. He found that the results of his models agreed closely with what was found in alligator literature and observations. The model mass of 131 kg was very similar to the recorded mass of 129.3 kg in the literature for a slightly smaller individual. In addition, the position of the model at equilibrium, and the sequence of the model as it returns to equilibrium after being submerged are very similar to observations made of live alligators at equilibrium. These findings lend support to the validity of the modeling method (Henderson, 2003).

RESEARCH OBJECTIVE

The overall research objective of this thesis study is to create accurate body shape reconstructions for plesiosaur genera (*Cryptoclidus*, *Muraenosaurus*, and *Tatenectes*) that have a range of cross-sectional body shapes in order to understand how body shape impacts stability and buoyancy. In addition to creating reconstructions, the method of vertebral curving in plesiosaurs will be studied. In some animals, such as primates, spinal curving is caused by wedge-shaped vertebrae, however, it is predicted that the rhomboidal shape of the vertebrae cause the curvature in plesiosaurs. Using

measurements from each vertebra, the correlation between wedged and rhomboidal vertebrae and spinal curvature will be evaluated.

The hydrodynamic properties of *Tatenectes*, *Cryptoclidus*, and *Muraenosaurus* will be predicted through the use of computer modeling techniques modified from Henderson's 2006 method. In particular, the passive recovery of the models to equilibrium after submersion, recovery from a lateral roll, and the effect of lung deflation on buoyancy control will be investigated. Finally, predictions on the habitats and feeding methods of the three plesiosaurs will be made based on their body shapes and hydrodynamic properties.

Chapter 2. Plesiosaur Reconstructions

INTRODUCTION

Before any work could be done on computer models of plesiosaur hydrodynamic properties, body shape reconstructions in lateral and cross-sectional views had to be created. These new reconstructions were necessary because if there are not precise reconstructions based on the fossil remains, there will be errors introduced to the modeling process and the results will not be accurate.

The body shape reconstructions were created based on measurements and photographs taken from the fossil remains of three plesiosaur genera, *Tatenectes*, *Muraenosaurus*, and *Cryptoclidus*. The study animals were chosen because, according to the literature and previous reconstructions, they cover the known range of plesiosaur cross-sectional body shapes from dorsoventrally compressed to laterally compressed (Andrews, 1910; Brown, 1981; O’Keefe et al., 2011) and do so within one clade (Ketchum and Benson, 2010). More detailed descriptions of the three genera, along with information regarding their taxonomic relationships, stratigraphic distributions, and temporal distributions, are included in Chapter 1.

MATERIALS AND METHODS

Materials

The following specimens were used to create skeletal reconstructions: USNM 536974, dorsal vertebrae, sacral vertebrae, pelvic girdle, dorsal ribs, and gastralia of *Tatenectes laramiensis*; NHM R.2863, pectoral and dorsal vertebrae of *Muraenosaurus leedsii*; NHM R.2860, cervical vertebrae, pectoral vertebrae, dorsal vertebrae, sacral

vertebrae, dorsal ribs, and gastralium of *Cryptoclidus eurymerus*; NHM R.2616, pectoral girdle and pelvic girdle of *Cryptoclidus eurymerus*.

Photographs

All photographs were taken using a Canon Eos 30, 8.6 megapixel camera that was set up on a tripod. The camera was positioned on the tripod using an attached leveling tool. The 50-110 mm zoom lens was used. A 10 cm scale bar was photographed alongside all of the specimens. The scale bar was slightly distorted in a few of the images; however, the distortion was not great enough to affect the image scaling process.

Vertebrae—In *Tatenectes*, 19 dorsal and three sacral vertebrae were photographed in left lateral view. The vertebrae were propped up in a lateral position using foam blocks. Photographs of two cervical, three pectoral, 20 dorsal, and one sacral vertebrae of *Cryptoclidus* were taken in left lateral, anterior, and dorsal views. For *Muraenosaurus*, two pectoral and 20 dorsal vertebrae were shot in left lateral, anterior, and dorsal views.

Ribs—Pictures were taken in anterior view for the dorsal ribs of *Cryptoclidus*. The series of dorsal ribs in *Muraenosaurus* was not complete or in order, making it impossible to determine where they would articulate along the vertebral column. Due to this, the photographs that were taken were not utilized in this study. *Tatenectes* rib images are from O’Keefe et al. (2011).

Gastralia—Photographs were shot of articulated *Cryptoclidus* gastralium bundles in anterior view. The gastralium photographed were from several points along the trunk region. As with the rib photographs, the *Muraenosaurus* gastralium images were not used

in this study due to their incomplete nature and the *Tatenectes* gastralium images are from O'Keefe et al. (2011).

Girdles—The left and right ilia, ischia, and pubes of *Tatenectes* were placed in articulation upside down to allow for the lateral view to be visible in the photograph. If the hip had been articulated dorsal side up, the lateral views would have been obscured by the foam that was used to prop up the bones. The photograph was later vertically flipped in Photoshop¹. The girdle was articulated by propping the individual bones up on foam, leaving about 1 cm between the bones to account for cartilage that would have been there in life. The articular surfaces were made to be parallel along the midline of the girdle. Once articulated, the pelvic girdle was shot in left and right lateral views. The individual bones were cut out using Photoshop. Due to the incomplete nature of several of the elements, a composite image was constructed consisting of the best preserved elements; the left ilium, left ischium and right pubis. The pelvic and pectoral girdles used in the *Cryptoclidus* reconstructions were reproduced from illustrations by Andrews (1910).

Vertebrae and Girdle Articulation

Photographs of the individual vertebra were cut out from their surroundings using Photoshop. The vertebrae for each genus were put in order on a new canvas and were scaled to one another using the 10cm scale bars from the original photographs. The angles of the vertebral faces, the articulations of the pre- and post- zygapophyses, and the position of the transverse processes were used to reconstruct the vertebral columns. Space of about 1 cm was left between each vertebra to account for the intervertebral disk that

¹ Photoshop is a registered trademark of Adobe Systems Incorporated. All rights reserved. The version used in this study is Adobe Photoshop Elements ver. 7.0.

would have been present in life. The width of the disks is known from vertebrae that were preserved in articulation where the region originally occupied by the intervertebral disk has been replaced by matrix.

The dorsal vertebrae of *Muraenosaurus* presented a problem. The vertebrae were not in order in the NHM collection and the vertebral number was not indicated on the fossils. To determine the order of the vertebrae, descriptions and drawings of the *Muraenosaurus* vertebral column and individual vertebrae from Andrews (1910) and Brown (1981) were studied for morphological clues of position. In addition, vertebra size and shape, face angles, and angles formed by the transverse processes and neural spine in anterior and dorsal views were used to order the vertebrae.

The pelvic girdle of *Tatenectes* was added to the composite image of the vertebral column and was scaled using the 10 cm scale bar from the original image. For *Cryptoclidus*, the original Andrews (1910) images were stated as 1/6th natural size. However, O’Keefe et al. (2011) added a 10cm scale bar to the image of the pelvic girdle, which was recalculated from measurements given in Andrews (1981). The image with the scale bar was utilized in order to increase the ease of scaling the girdle to the vertebral column. Information from the literature (Andrews, 1910; Brown, 1981) was used to help determine the angles that the girdles articulated to the vertebral column.

Centrum Angles

Vertebral Wedging—Measurements were taken in order to determine the wedging angle of each vertebra. The wedging angle is a ratio derived from an equation involving the differences in posterior and anterior vertebra heights and the vertebra length, as described below. This is a method that was developed to describe the wedged shaped

vertebra in primates. Wedging of adjacent vertebrae is responsible for the vertebral curving seen in primate spinal columns (Digiovanni et al., 1989; Whitcome et al., 2007).

In order to account for the differences in spinal column positions between primates and plesiosaurs, the dorsal and ventral centrum lengths and the dorsoventral centrum heights were measured instead of the anterior and posterior measurements used in Primates. All of the centra were measured (in mm) from photographs of the vertebrae in lateral view using the line measurement tool in an open source image processing software developed by the National Institutes of Health, ImageJ (Rasband, 2011). The measurements were recorded and the wedging angles were calculated in Excel² using the formula:

$$\text{Wedging} = 2 * \text{arc tan} \{[(\text{ventral length} - \text{dorsal length}) / 2] / \text{dorsoventral height}\}$$

This was modified from the formula developed by researchers to determine lordotic (ventral) and kyphotic (dorsal) spinal curvature in primates due to wedge shaped vertebrae (Digiovanni et al., 1989; Whitcome et al. 2007). Vertebrae with negative wedging angles are lordotic vertebrae and vertebrae with positive angles are kyphotic. As per Digiovanni et al. (1989), three adjacent vertebrae with wedging angles of 5 degrees or more were considered to represent a region of kyphotic curvature and three or more in a row with -5 degrees or fewer represented a lordotic curve.

In addition to the vertebral wedging due to differences in dorsal and ventral centrum lengths, differences in the anterior centrum heights, posterior centrum heights, and anteroposterior lengths of all centra were also examined to see if there was any correlation with spinal curvature. For the purpose of this paper, the resulting angles will

² Excel is a registered trademark of the Microsoft Corporation. All rights reserved. The version used in this study is Microsoft Excel 2003 (11.8328.8329) SP3.

be referred to as anteroposterior wedging angles. As with the dorsal and ventral centrum lengths, the anterior, posterior, and anteroposterior centrum heights were measured (in mm) from photographs of the vertebrae in lateral view using the line measurement tool in the ImageJ software (Rasband, 2011). The measurements were recorded and the wedging angles were calculated in Excel using the formula:

$$\textit{Anteroposterior Wedging} = 2 * \textit{arc tan} \{[(\textit{posterior height} - \textit{anterior height}) / 2] / \textit{Anteroposterior length}\}$$

This formula is almost identical to the formula presented by Digiovanni et al. (1989) except that it is taking into account the vertebral faces perpendicular to the ones used to determine lordotic and kyphotic vertebrae. An association between vertebrae with greater than 5 degrees or fewer than -5 degrees of anteroposterior wedging and regions of spinal curvature was investigated.

Anterior and Posterior Face Angles—Angle measurements were taken from the photographs of the *Tatenectes*, *Cryptoclidus*, and *Muraenosaurus* vertebrae in lateral view (Tables 2.1, 2.2, 2.3). Lines that approximated the anterior face, posterior face, and ventral margin of each vertebra were added using Photoshop. The angles between the anterior and ventral lines and between the posterior and ventral lines were measured to the nearest half degree using the angle measurement tool in the ImageJ software (Rasband, 2011) and recorded in Excel workbooks. In instances where one of the vertebral faces was broken, the best estimate of the face angle was measured. The data points from broken faces were marked with an asterisk (*) on the graphs (Figs. 2.1b, 2.2b, 2.3b) to indicate uncertainty of the measurement.

The angle measurements for *Cryptoclidus* were done a second time by Dr. O'Keefe to test for reproducibility. For the anterior vertebrae with torqued faces, the second set of measurements differed from the original measurements by up to three degrees in a few cases. For the vertebrae without torqued faces, the measurements were reproducible within one degree. In the cases where the angle measurements differed, the values from the second set of measurements were used. Despite the slight differences in the anterior vertebrae measurements, the patterns seen in the original and second set of measurements were the same. Graphs of the anterior and posterior angle measurements for each genus were generated using Excel in order to see how centrum shape changes across the vertebral column (Figs. 2.1b, 2.2b, 2.3b).

Rib Orientation

To determine the angles of articulation of the ribs, the shape of the articular surface of the transverse process were measured. The posteroventral slant of the articular surface was measured from the photograph of the vertebra in left lateral view (Fig. 2.1a). Then the posteromedial angle of the transverse process articular surface was measured from the dorsal view photograph (Fig. 2.1b). Once those two angles were measured, calculations were done to find the length that the rib would appear to be in anterior view when articulated (Fig. 2.1c). This was accomplished by taking the cosine of the posteroventral slant to determine the degree to which the rib would appear shortened in anterior view. The cosine of the posteromedial slant was calculated next in order to find the medial migration of the rib tip that would be observed in anterior view.

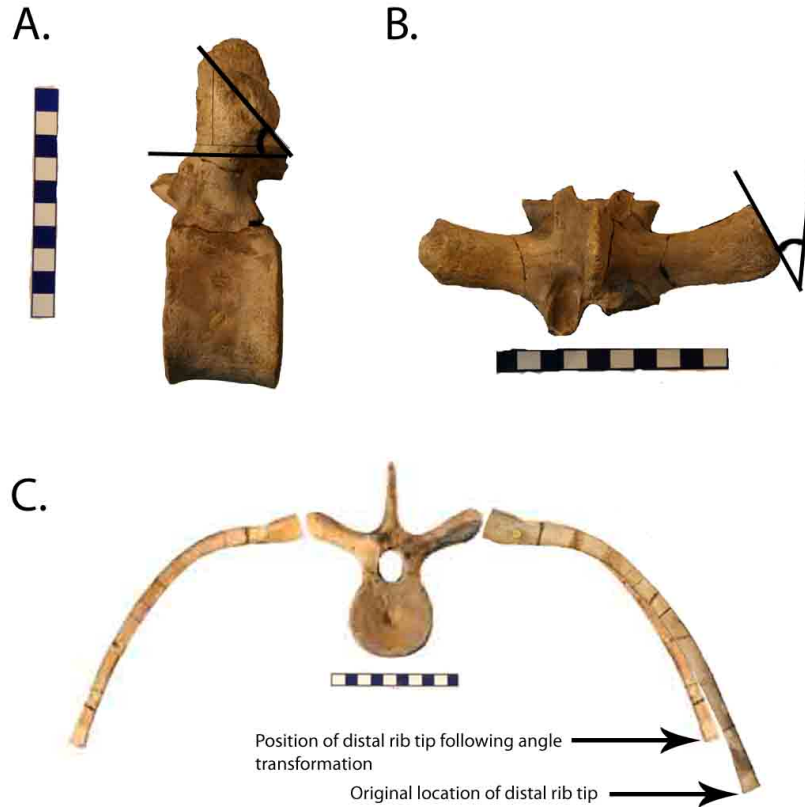


Figure 2.1. *Cryptoclidus* rib orientation. **A.** Vertebra in left lateral view showing the posteroventral slant of the articular surface. **B.** Vertebra in dorsal view showing the posteromedial angle of the articular surface of the transverse process. **C.** Vertebra and ribs showing the location of the distal rib tip pre- and post-angle transformation.

Transverse Cross Section

The cross section of *Cryptoclidus* was done using the 11th dorsal vertebra. It was chosen due to its location in the mid-trunk region of the animal, its completeness, and the lack of restoration to the transverse processes. The corresponding left rib was articulated at the orientation determined by the method described in the previous section. In order to make the rib appear the correct size in the articulated anterior view, the free transform function of Photoshop was used to move the tip of the rib dorsomedially. The rib image was then copied and flipped horizontally to form a mirror image to use on the other side of the cross section. A complete, articulated bundle of gastralia from the mid-trunk region

was added to the composite image and the size was scaled to match the vertebra. The location of the gastralia in the cross section was determined by lining up the tips of the gastralia with the distal rib tips so they formed a smooth curve. However, the gap between the gastralia and the distal tip of the ribs is artificial due to an error in the articulation of the gastralia that caused them to be shortened in transverse section. The cross section of *Tatenectes* was reproduced from O’Keefe et al. (2011). Due to the uncertainty of rib and gastralium positions along the vertebral column of *Muraenosaurus*, a reconstruction of the transverse cross section was not done.

RESULTS

As expected from previous reconstructions (Andrews, 1910; Brown, 1981; O’Keefe et al., 2011), *Tatenectes* had the flattest vertebral profile (Fig. 2.2), followed by *Cryptoclidus* (Fig. 2.3), then *Muraenosaurus* (Fig. 2.4). The centra angle graphs (Figs. 2.2, 2.3, 2.4) show that there is a correlation between spinal curvature and centrum shape. The most rhomboidal vertebrae (the vertebrae with the greatest difference between the anterior and posterior angles) are associated with the areas of the greatest degree of spinal curvature. The less rhomboidal vertebrae are associated with flatter areas of the vertebral column and areas where the curvature is gradual. On the centra angle graphs (Figs. 2.2, 2.3, 2.4), regions where the posterior angles are greater than the anterior angles represent upward spinal curvature. Conversely, regions with anterior angles that are greater than their posterior counterparts are areas of downward curvature. Changes in the overall spinal curvature are represented by intersections of the anterior and posterior angle lines on the graphs (Figs. 2.2, 2.3, 2.4).

In contrast to the condition seen in Primates, plesiosaur spinal curvature is not associated with wedging of the vertebrae. In the three plesiosaur genera studied, there was a combination of lordotic and kyphotic vertebrae. Unlike the lordotic and kyphotic curves seen in the human specimens discussed in Whitcome et al. (2007) and Digiovanni et al. (1989), there were no instances of three adjacent vertebrae with wedging angles greater than five degrees in the plesiosaur genera (Tables 2.4, 2.6, 2.8). There was also no clear association between anteroposterior wedging and spinal curvature (Tables 2.5, 2.7, 2.9) with the exception of the curve seen in the posterior region of the *Tatenectes* spinal column. This suggests that it is the rhomboidal vertebral shape rather than any vertebral wedging is the cause of curvature along the spinal column.

Tatenectes is flat for the majority of the dorsal series, with the only notable curve occurring in the posteriormost dorsal vertebrae (Fig. 2.2a). This reconstruction is corroborated by the metric data from the centra (Fig. 2.2b). There is little difference between the anterior and posterior angles until the 13th dorsal vertebra, which is the start of the downward curve. The anterior and posterior angles become similar again at the beginning of the sacral series, marking the end of the downward curve.

In *Cryptoclidus*, there is a steep upward curve from the posterior cervical vertebrae to the second dorsal vertebra. The posterior dorsal vertebrae have a gently sloping downward curve (Fig. 2.3a). A qualitative comparison of reconstructions shows that this new reconstruction has a slightly higher vertebral profile than the reconstruction by Brown (1981). However, the posterior curvature is very similar, giving the animal a flatter profile than the Andrews (1910) reconstruction. It is unclear how the curvature of the anterior dorsal vertebrae of the new reconstruction compares to Brown's (1981), as

the anterior dorsals are obstructed by the forelimb in Brown's reconstruction. The anterior curve is a little steeper and the highest point of the spinal column is more anterior in the new reconstruction in comparison to the one in Andrews (1910).

The *Cryptoclidus* centra are rhomboidal from the end of the cervical series through the second dorsal vertebra, with the posterior angles being markedly higher than the anterior angles. This corresponds with the steep upward curve seen in the spinal reconstruction. The gentle downward slope of the posterior dorsal vertebrae corresponds with the centra where the anterior angles are slightly larger than the posterior angles (Fig. 2.3a,b).

The curvature of the *Muraenosaurus* reconstruction is very similar to the reconstruction by Andrews (1910). Both reconstructions have steep anterior and posterior curves in the dorsal vertebrae, resulting in a high vertebral profile. The *Muraenosaurus* centra data from the anterior dorsal vertebrae does not correspond as well with the vertebral reconstruction as it did in *Tatenectes* and *Cryptoclidus*. This finding suggests that some of the anterior vertebral column is incorrectly articulated. As mentioned in the methods section, the exact order of the *Muraenosaurus* dorsal vertebrae is unsure. It is likely that any articulation errors in the anterior dorsals are due to misplaced vertebrae. In contrast to the anterior region, the centra angles of the central and posterior vertebrae reflect the downward curve seen in the reconstruction.

The reconstruction of *Cryptoclidus* in transverse cross section (Fig. 2.5a) is an almost perfect circle. This is in stark contrast to the oblate transverse section seen in *Tatenectes* (Fig. 2.5b). The new *Cryptoclidus* transverse section is intermediate between

the more dorsoventrally compressed cross section from Henderson (2006) and the slightly more circular cross section from O’Keefe et al. (2011).

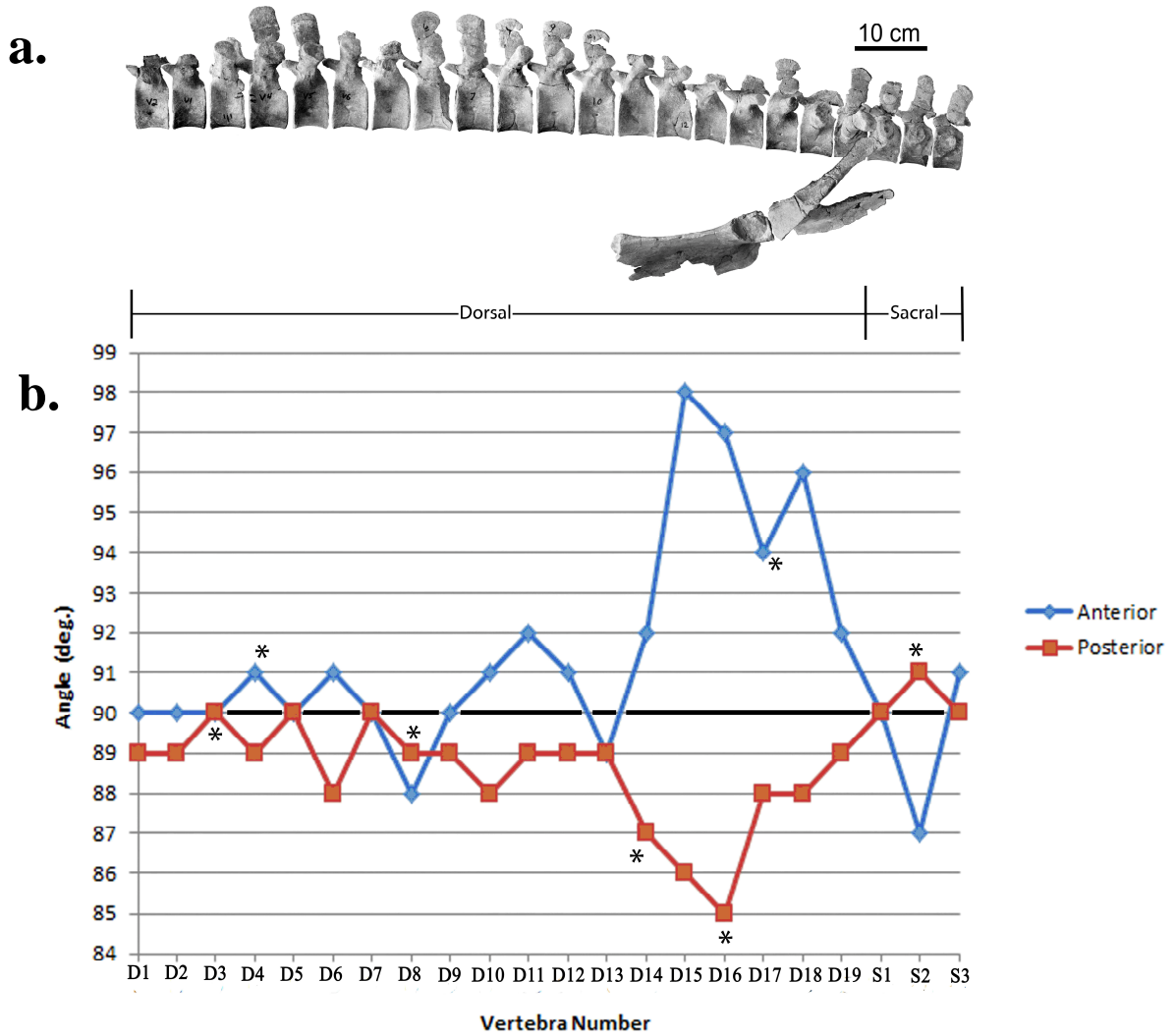


Figure 2.2. *Tatenectes* reconstruction. **a.** Articulated vertebral column with pectoral girdle. Girdle reproduced from O’Keefe et al. (2011). **b.** Graph of the centra angles. Anterior to the left. *Broken vertebral face.

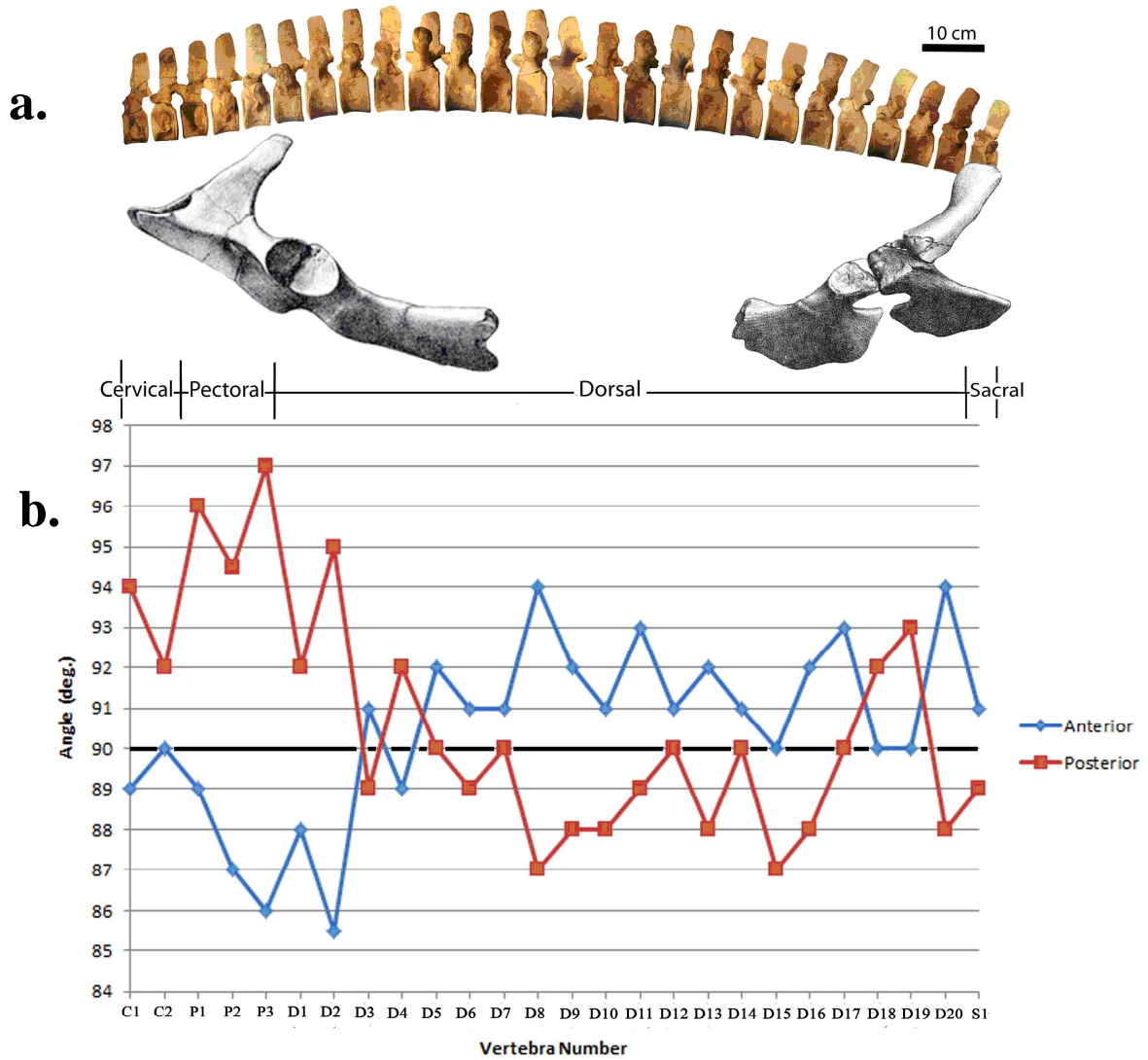


Figure 2.3. *Cryptoclidus* reconstruction. **a.** Articulated vertebral column with pelvic and pectoral girdles. Girdles reproduced from Brown (1910). **b.** Graph of the centra angles. Anterior to the left.

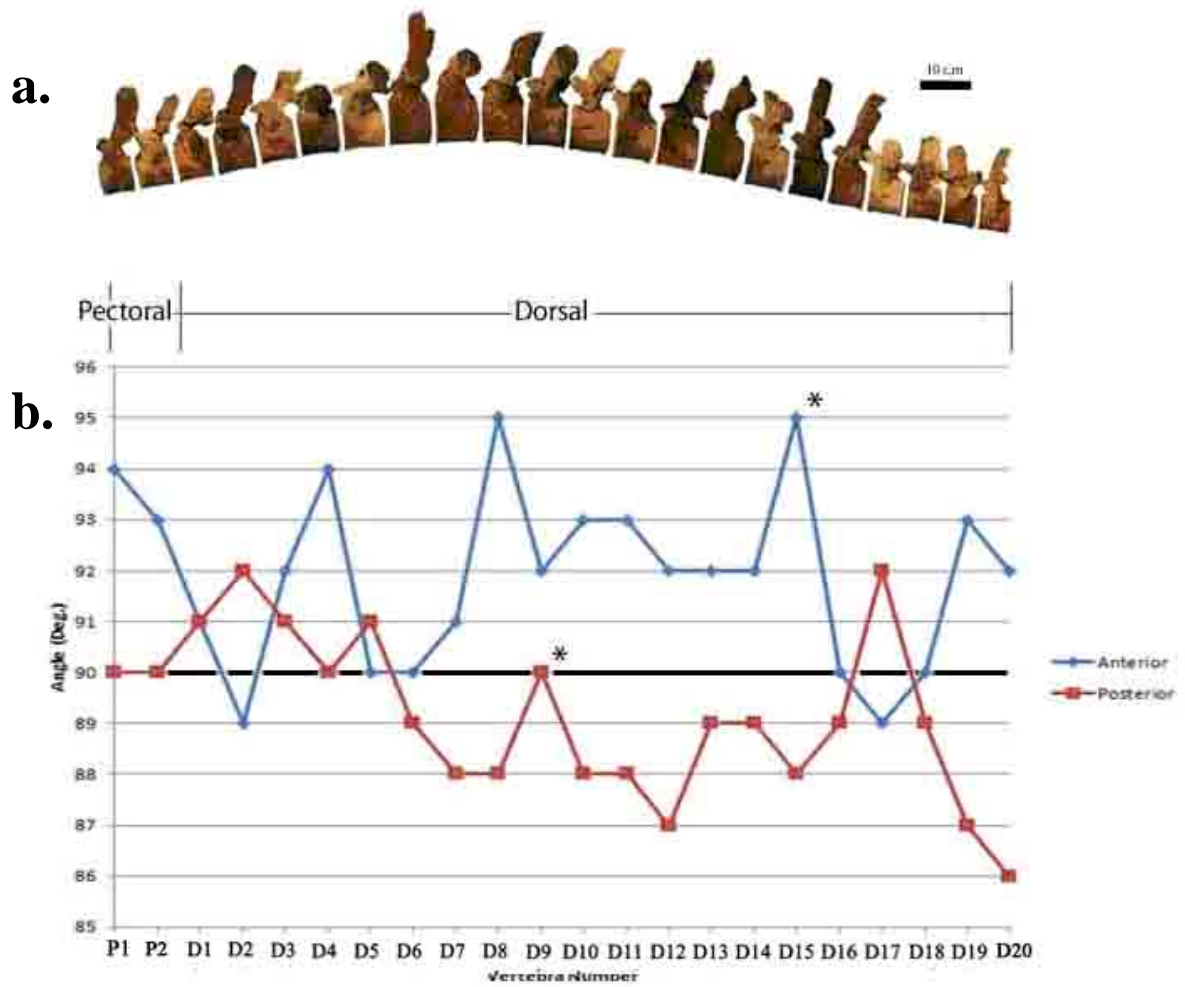


Figure 2.4. *Muraenosaurus* reconstruction. a. Articulated vertebral column. **b.** Graph of the centra angles. Anterior to the left. *Broken vertebral face.

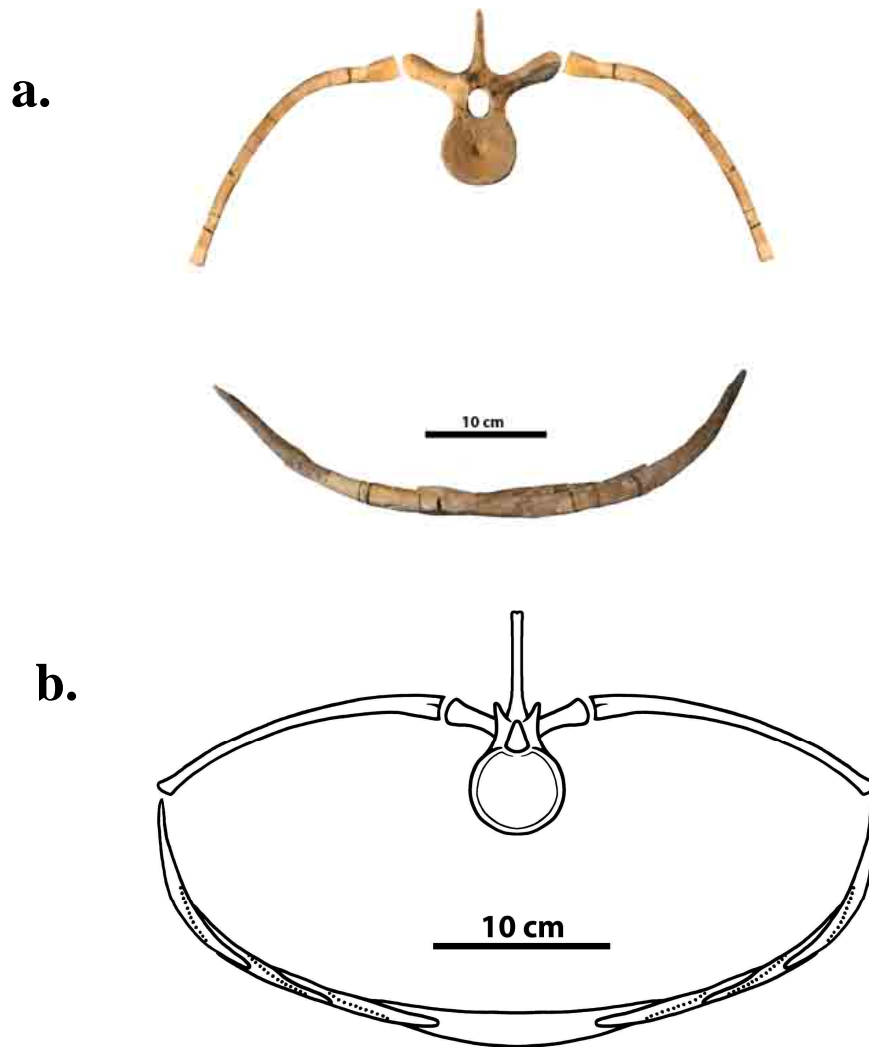


Figure 2.5. Transverse cross sections. a. *Cryptoclidus eurymerus* cross section. **b.** *Tatenectes laramiensis* cross section. Reproduced from O’Keefe et al. (2011).

Table 2.1. *Tatenectes* centra angles.

Vertebra Number	Anterior Angle (deg.)	Posterior Angle (deg.)
D1	90	89
D2	90	89
D3	90	90
D4	91	89
D5	90	90
D6	91	88
D7	90	90
D8	88	89
D9	90	89
D10	91	88
D11	92	89
D12	91	89
D13	89	89
D14	92	87
D15	98	86
D16	97	85
D17	94	88
D18	96	88
D19	92	89
S1	90	90
S2	87	91
S3	91	90

Table 2.2. *Cryptoclidus* centra angles.

Vertebra Number	Anterior Angle (deg.)	Posterior Angle (deg.)
C31	89	94
C32	90	92
P1	89	96
P2	87	94.5
P3	86	97
D1	88	92
D2	85.5	95
D3	91	89
D4	89	92
D5	92	90
D6	91	89
D7	91	90
D8	94	87
D9	92	88
D10	91	88
D11	93	89
D12	91	90
D13	92	88
D14	91	90
D15	90	87
D16	92	88
D17	93	90
D18	90	92
D19	90	93
D20	94	88
S1	91	89

Table 2.3. *Muraenosaurus* centra angles.

Vertebra Number	Anterior Angle (deg.)	Posterior Angle (deg.)
P1	94	90
P2	93	90
D1	91	91
D2	89	92
D3	92	91
D4	94	90
D5	90	91
D6	90	89
D7	91	88
D8	95	88
D9	92	90
D10	93	88
D11	93	88
D12	92	87
D13	92	89
D14	92	89
D15	95	88
D16	90	89
D17	89	92
D18	90	89
D19	93	87
D20	92	86

Table 2.4. *Tatenectes* wedging angles.

Vertebra Number	Dorsal Width (mm)	Ventral Width (mm)	Dorsoventral Height (mm)	Wedging Angle	Vertebra Shape
D1	42.5	44.6	53.2	2.261382	Kyphotic
D2	43.6	42.5	52.2	-1.20734	Lordotic
D3	43.5	47.3	59.1	3.682724	Kyphotic
D4	Broken	50.5	Broken	N/A	N/A
D5	45.9	46.8	57.0	0.904651	Kyphotic
D6	44.1	32.8	53.9	-11.9682	Lordotic
D7	44.1	49.0	64.0	4.384567	Kyphotic
D8	Broken	Broken	56.5	N/A	N/A
D9	46.8	47.3	59.1	0.484733	Kyphotic
D10	45.7	45.8	57.6	0.099472	Kyphotic
D11	50.0	46.8	54.4	-3.36937	Lordotic
D12	46.5	45.6	51.2	-1.00713	Lordotic
D13	45.6	47.2	52.0	1.762808	Kyphotic
D14	Broken	Broken	47.2	N/A	N/A
D15	39.8	40.2	43.7	0.524443	Kyphotic
D16	44.8	43.1	42.4	-2.29693	Lordotic
D17	41.6	40.9	44.8	-0.89523	Lordotic
D18	43.3	43.5	39.2	0.292325	Kyphotic
D19	Broken	42.1	43.3	N/A	N/A
S1	41.3	40.2	46.6	-1.35241	Lordotic
S2	37.3	Broken	48.4	N/A	N/A
S3	37.0	34.9	50.5	-2.38225	Lordotic

Table 2.5. *Tatenectes* anteroposterior wedging angles.

Vertebra Number	Anterior Height (mm)	Posterior Height (mm)	Anteroposterior Length (mm)	Wedging Angle
D1	59.7	57.0	44.1	-3.50681
D2	59.1	57.5	43.5	-2.10719
D3	59.1	59.1	46.2	0
D4	Broken	47.8	48.4	N/A
D5	57.0	47.8	46.2	-11.3721
D6	58.1	56.5	45.7	-2.00577
D7	61.8	62.9	48.4	1.302121
D8	58.1	57.0	50.0	-1.26046
D9	58.1	61.3	46.8	3.916135
D10	60.2	58.1	45.7	-2.63238
D11	60.2	61.3	46.8	1.346634
D12	54.3	55.9	46.4	1.975521
D13	55.9	54.8	46.8	-1.34663
D14	51.1	52.7	44.2	2.073829
D15	43.0	44.2	39.7	1.731731
D16	43.0	47.8	43.3	6.345003
D17	48.0	50.5	39.9	3.588787
D18	37.6	51.2	42.6	18.13859
D19	Broken	48.0	42.1	N/A
S1	52.8	49.3	39.0	-5.13848
S2	51.5	Broken	Broken	N/A
S3	51.2	51.5	34.1	0.504065

Table 2.6. *Cryptoclidus* wedging angles.

Vertebra Number	Dorsal Width (mm)	Ventral Width (mm)	Dorsoventral Height (mm)	Wedging Angle	Vertebra Shape
C31	39.2	36.9	47.6	-2.76796	Lordotic
C32	35.9	36.9	48.7	1.176463	Kyphotic
P1	43.5	36.3	53.0	-7.77164	Lordotic
P2	41.7	39.3	55.3	-2.48623	Lordotic
P3	44.0	39.6	52.1	-4.83593	Lordotic
D1	44.1	41.7	54.6	-2.51809	Lordotic
D2	46.4	44.3	56.0	-2.14834	Lordotic
D3	44.8	43.2	53.7	-1.70701	Lordotic
D4	48.1	44.9	55.3	-3.31456	Lordotic
D5	46.5	48.0	59.2	1.451674	Kyphotic
D6	47.2	47.2	58.4	0	N/A
D7	48.0	46.4	62.4	-1.46904	Lordotic
D8	45.6	44.8	65.6	-0.69872	Lordotic
D9	48.8	48.1	64.1	-0.62569	Lordotic
D10	49.6	48.1	60.8	-1.41348	Lordotic
D11	49.8	45.7	63.4	-3.70396	Lordotic
D12	46.6	47.4	61.0	0.751409	Kyphotic
D13	46.7	49.2	59.5	2.407032	Kyphotic
D14	47.0	44.9	58.7	-2.04955	Lordotic
D15	48.4	50.1	57.4	1.696789	Kyphotic
D16	49.5	47.7	54.1	-1.90615	Lordotic
D17	47.7	44.5	50.1	-3.65837	Lordotic
D18	49.0	45.5	50.4	-3.97728	Lordotic
D19	47.7	43.8	52.1	-4.28693	Lordotic
D20	43.9	43.7	49.9	-0.22964	Lordotic
S1	42.3	42.9	47.7	0.720692	Kyphotic

Table 2.7. *Cryptoclidus* anteroposterior wedging angles.

Vertebra Number	Anterior Height (mm)	Posterior Height (mm)	Anteroposterior Length (mm)	Wedging Angle
C31	48.6	46.4	35.5	-3.54959
C32	47.7	48.2	35.0	0.818497
P1	52.7	50.0	35.5	-4.35561
P2	55.5	53.6	39.1	-2.78365
P3	57.3	51.4	39.5	-8.54225
D1	56.4	57.3	40.0	1.289101
D2	60.5	55.9	42.7	-6.16642
D3	56.8	54.5	41.4	-3.18228
D4	54.1	56.4	44.1	2.987538
D5	60.0	63.2	45.0	4.072651
D6	61.4	59.1	47.7	-2.76215
D7	60.5	57.7	45.0	-3.56392
D8	62.3	61.8	44.5	-0.64377
D9	62.3	65.5	45.0	4.072651
D10	61.4	60.5	46.4	-1.11131
D11	60.9	61.8	44.1	1.169261
D12	62.3	65.0	45.9	3.369369
D13	69.5	60.9	46.4	-10.5892
D14	63.6	59.1	42.7	-6.03262
D15	61.8	58.6	45.5	-4.02793
D16	59.5	58.6	44.1	-1.16926
D17	53.6	56.4	41.8	3.836561
D18	54.1	53.6	43.6	-0.65705
D19	54.1	52.3	43.2	-2.38698
D20	51.3	51.8	40.5	0.707346
S1	52.4	51.8	43.9	-0.78307

Table 2.8. *Muraenosaurus* wedging angles.

Vertebra Number	Dorsal Width (mm)	Ventral Width (mm)	Dorsoventral Height (mm)	Wedging Angle	Vertebra Shape
P1	61.6	58.4	65.7	-2.79011	Lordotic
P2	64.1	61.2	64.8	-2.56374	Lordotic
D1	66.5	65.2	70.8	-1.05201	Lordotic
D2	67.5	72.4	74.8	3.751992	Kyphotic
D3	69.1	66.8	77.3	-1.70466	Lordotic
D4	72.8	70.5	79.5	-1.6575	Lordotic
D5	66.8	73.2	81.9	4.47505	Kyphotic
D6	74.7	75.6	87.2	0.59135	Kyphotic
D7	74.8	74.7	80.9	-0.07082	Lordotic
D8	71.5	72.3	79.2	0.57874	Kyphotic
D9	70.5	70.9	81.1	0.282593	Kyphotic
D10	73.2	69.5	77.7	-2.72786	Lordotic
D11	69.7	70.6	83.5	0.617553	Kyphotic
D12	69.2	70.9	78.7	1.237599	Kyphotic
D13	72.5	69.1	77.7	-2.50675	Lordotic
D14	70.4	71.9	77.6	1.107487	Kyphotic
D15	67.3	68.1	70.9	0.64649	Kyphotic
D16	62.5	66.8	65.3	3.77156	Kyphotic
D17	60.4	61.9	61.7	1.39286	Kyphotic
D18	60.4	60.9	62.5	0.458364	Kyphotic
D19	60.5	58.8	56.4	-1.72687	Lordotic
D20	55.9	56.5	58.8	0.584646	Kyphotic

Table 2.9. *Muraenosaurus* anteroposterior wedging angles.

Vertebra Number	Anterior Height (mm)	Posterior Height (mm)	Anteroposterior Length (mm)	Wedging Angle
P1	62.0	66.7	57.1	4.713455
P2	64.8	68.9	62.9	3.73338
D1	76.9	74.3	64.3	-2.31647
D2	81.2	80.0	71.5	-0.96158
D3	81.7	77.1	66.8	-3.94396
D4	80.0	81.7	72.9	1.336055
D5	89.2	79.6	74.5	-7.37289
D6	88.7	84.0	76.1	-3.53751
D7	86.8	86.0	70.1	-0.65387
D8	86.0	89.3	72.1	2.621957
D9	84.0	84.0	69.3	0
D10	84.3	83.6	70.0	-0.57295
D11	79.2	83.6	68.4	3.684423
D12	82.9	81.3	69.5	-1.31898
D13	84.0	77.4	70.4	-5.36755
D14	79.1	80.4	71.5	1.041713
D15	Broken	72.4	Broken	N/A
D16	72.1	70.4	65.3	-1.49154
D17	67.3	65.3	63.9	-1.79315
D18	69.1	63.1	62.4	-5.50497
D19	63.7	61.1	58.3	-2.55479
D20	67.1	61.3	57.3	-5.79463

DISCUSSION

The spinal reconstructions ranged from a low spinal profile in *Tatenectes* to a high profile in *Muraenosaurus* with *Cryptoclidus* having an intermediate spinal profile. The results are in accordance with previous reconstructions (Andrews, 1910; Brown, 1981; O’Keefe et al., 2011). However, there were some differences between the new reconstructions of *Cryptoclidus* with reconstructions of Andrews (1910) and Brown (1981). The new *Cryptoclidus* reconstruction has a spinal profile that is intermediate to the ones seen in Brown (1981) and Andrews (1910). The highest point of the spinal curve is also located more anteriorly. The new cross-sectional reconstruction also differs from

past reconstructions, with a shape that is intermediate between the oblate reconstruction seen in Henderson (2006) and the circular shape from O'Keefe et al. (2011). There are also some differences between the new *Muraenosaurus* reconstruction and Andrew's (1910) reconstruction. However, they are very similar overall and the differences are probably due to inaccurate vertebral ordering in the new reconstruction.

In all three plesiosaur taxa, the curvature of the spine was due to the rhomboidal nature of the vertebrae it the most rhomboidal vertebrae corresponding with the regions of greatest curvature. In primates, wedged shaped vertebrae are the cause of spinal curvature. However in the plesiosaurs studied, there was no correlation between either the wedging angles or the anteroposterior wedging angles and curvature, with one exception. In a portion of the posterior curve of *Tatenectes* from vertebrae 16 to18, there are consecutive, large anteroposterior wedging angles (Table 2.5). This region corresponds with both the steepest part of the spinal curve and the most rhomboidal vertebrae in the series. This indicates that in some plesiosaur taxa, anteroposterior wedging of the vertebrae, as well as rhomboidal vertebrae, may contribute to spinal curvature.

Chapter 3. Plesiosaur Buoyancy and Stability

INTRODUCTION

In order to test the influence of cross-sectional shape on plesiosaur buoyancy and stability, 3-D virtual models of plesiosaurs with varying shapes were run through a series of tests following Henderson (2006). The tests include the ability of the model to passively return to equilibrium at the water surface after being submerged, the effect of lung deflation on buoyancy, and the return to equilibrium from a lateral roll. It is predicted that animals that are more stable at the surface would be suited for shallow-marine environments, whereas animals that are unstable at the water surface would have inhabited deep-water environments as is the case in extant whales (Fish, 2002).

Computer models were made for *Tatenectes*, *Cryptoclidus*, and *Thalassomedon*. The body shapes for *Tatenectes* and *Cryptoclidus* were based on the spinal reconstructions presented in Chapter 2. Modeling was not done for *Muraenosaurus* because of the likelihood of errors in the reconstruction due to the uncertainty of vertebra order discussed in Chapter 2. The *Thalassomedon* model and test results from Henderson (2006) were used in place of *Muraenosaurus*. *Thalassomedon* is another deep-bodied elasmosauromorph morphologically similar to *Muraenosaurus*, however, *Muraenosaurus* is slightly more deep-bodied and *Thalassomedon* has a longer neck. Due to this switch, the study no longer included the entire range of known plesiosaur body shapes. However, it was still possible to investigate differences in the hydrodynamic properties of flat-bodied and deep-bodied taxa and the implications for their ecology and behavior.

MATERIALS AND METHODS

Materials

The lateral views of the trunk regions of *Tatenectes* and *Cryptoclidus* from Chapter 2 were used to construct models used in the buoyancy and stability tests. The neck and tail in lateral view and the dorsal view of *Tatenectes* were modeled based on the reconstruction by O’Keefe et al. (2011). The neck and tail length suggested for *Tatenectes* were estimates based on related taxa since there are no specimens with preserved cervical and caudal series. For the *Cryptoclidus* model, the neck and tail in lateral view were based on Brown’s (1981) reconstruction. The dorsal view of *Cryptoclidus* was from Henderson’s 2006 publication on plesiosaur buoyancy. As mentioned previously, the *Thalassomedon* models were also taken from Henderson (2006).

Methods

Models—The computer models were made by Dr. Henderson of the Royal Tyrell Museum using the techniques that he developed and described in detail in his 1999, 2003, and 2006 publications. The following is an overview of his methods.

In order to create the models, the lateral view reconstructions of the study animals were put onto graphs with a vertical y-axis and longitudinal x-axis. The reconstructions in dorsal view were put onto graphs with a longitudinal x-axis and horizontal z-axis. Lines were then added, which crossed the dorsal and ventral edges of the lateral reconstructions and the left and right margins of the dorsal reconstructions (Fig. 3.1a). The number of lines added to each body region was determined by the degree of curvature in the region. Areas with a high degree of curvature required more lines in order to be accurately

represented than did flat regions of the reconstruction. The points where the lines intersected the outline in lateral and dorsal views were recorded and plotted in 3-D space, resulting in a series of elliptical slabs. Lines were then added that connected the anterior and posterior margin of each ellipse at constant intervals around the edge of the slice, to form a hollow mesh made up of a series of elliptical slabs of varying thickness (Fig. 3.1b). This hollow mesh defined the 3-dimensional shape of each model.

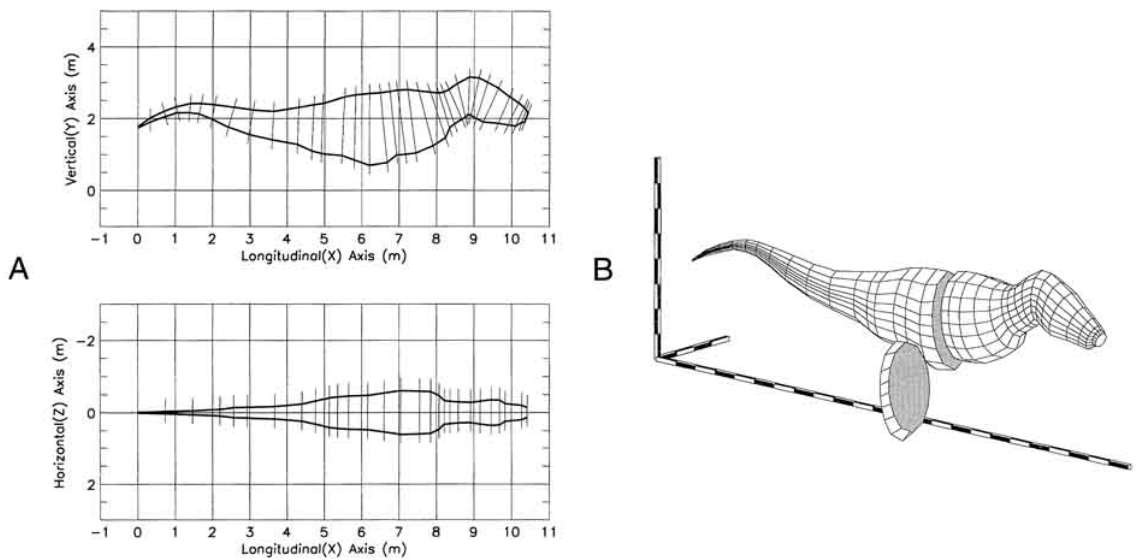


Figure 3.1. 3D slicing method. **A.** Graphs showing the lines crossing the outline of a *Tyrannosaurus rex* in lateral and dorsal views. **B.** Resulting 3D mesh with one slab removed. (Figure from Henderson, 1999).

In order to allow for precise computations of volume and center of mass (CM), all of the elliptical slabs in the model were further divided into 8 subslabs along the transverse plane. The volume of each subslab was calculated using the double integration:

$$volume_n = \int \int_R \{f_{top}(x, z) - f_{bottom}(x, z)\} dx dz$$

where R is the elliptical region at the midpoint of the n^{th} subslab and $f_{top}(x, z)$ and $f_{bottom}(x, z)$ are linear equations that define the top and bottom subslice that bound the n^{th} subslab. Once the subslab volumes are known, the volume of each slab was computed by summing its 8 subslab volumes. The volume of the entire model was determined by adding together the volumes of the individual slabs.

To find the CM of the model, the CM of each slab was first calculated. For any given elliptical slab, the CM was equal to the product of the centroid (geometric center) of the slab and its mass. To determine of the mass of the slab, the previously calculated slab volume was multiplied by the density of the tissue (assumed to be 1,050 g/l based on published values of tissue densities for extant taxa). Once the CM of each slab had been found, the CM of the body was calculated using the equation:

$$body_CM \begin{bmatrix} x \\ y \end{bmatrix} = \frac{\sum_{m=0}^{M-1} slab_mom \begin{bmatrix} x \\ y \end{bmatrix}_m}{\sum_{m=0}^{M-1} slab_mass_m}$$

where $\sum_{m=0}^{M-1} slab_mom \begin{bmatrix} x \\ y \end{bmatrix}_m$ is the sum of the moment of the vectors of each slab with respect to the x- and y-axes. Since plesiosaurs have bilateral symmetry, the CM has no lateral (z-axis) component and lies within the sagittal plane.

Addition of Lungs—Lungs with a volume equal to 9.8% of the total body volume and a nil density were incorporated into the models. The volume used for the lungs falls within range of known reptile lung volumes (8% - 10%). The lung volume of 9.8% that was used is on the high end for reptiles and was chosen because it is similar to the high lung volumes observed in extant aquatic reptiles (Henderson, 2006). The lungs

were placed anterodorsally in the trunk region of each model, in a position similar to the lung position observed in extant turtles and alligators (Fig. 3.2).

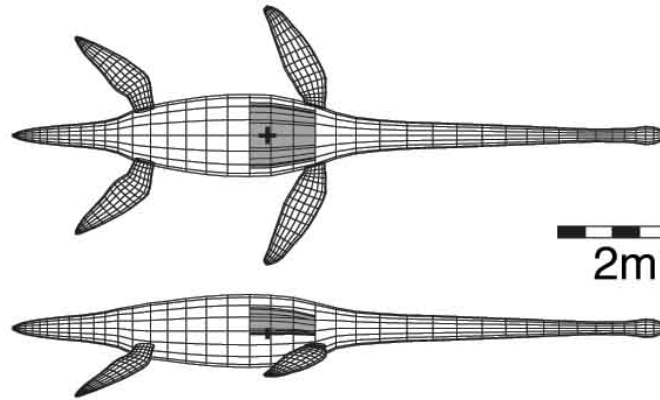


Figure 3.2. Lung position. The dark grey area in the anterior region of the trunk represents the lung positioning within *Thalassomedon*. The ‘+’ represents the location of the CM. (Figure from Henderson, 2006).

The addition of nil density lungs shifts the CM that was found for the body alone.

The adjusted CM of the body plus lungs was calculated with the equation:

$$Model_CM = \frac{body_CM \begin{bmatrix} x \\ y \end{bmatrix} \cdot body_mass + lung_CM \begin{bmatrix} x \\ y \end{bmatrix} \cdot lung_mass}{body_mass + lung_mass}$$

where the CM of the lungs was calculated from the lung subslabs using the same method as the original body CM calculation.

Gravitational and Buoyant Force Measurements—In order to perform the necessary calculations for determining the buoyant and gravitational forces acting on the models during the tests, the mesh models were resampled. Resampling was necessary since the original model consisted of slabs with variable thickness and the equations for

the buoyant and gravitational forces require a constant slab thickness. The resampled models were comprised of 100 uniformly thick disks of differing volumes.

The volume, density, and mass of each of the body disks were calculated. In the region containing the lungs, the density of each disk was found by subtracting the volume of the lung disk from the total volume of the body disk. The density of each disk was determined by multiplying the computed residual volume by the density of the tissue (1,050 g/l) and dividing the product by the full volume of the disk.

The force of gravity acting through the center of mass was expressed by the equation:

$$F_{\text{gravity}} = -g \sum_{m=0}^{M-1} \text{mass}_m$$

where the gravitational acceleration (g) is equal to 9.81 m/s^2 and mass_m is the mass of the m^{th} disk. The buoyancy force, which counteracts the force of gravity, was also determined for each disk. If a disk was fully submerged, the buoyant force was equal to the volume of water that it displaced. However, in the cases where the disks were only partially submerged (as is the case when the models are at equilibrium), only the submerged portion of the disk was taken into account. The buoyant force for the model as a whole was calculated by summing the submerged area of all the disks and multiplying that value by the uniform disk thickness, the density of sea water (1026 g/l), and the gravitational acceleration (9.81 m/s^2).

The buoyant torque was also taken into consideration. The buoyant torque is responsible for rotation about an axis perpendicular to the sagittal plane of the model. Rotation about the x-axis (lateral roll) was only taken into consideration in the recovery

from wave action test and will be addressed later. The buoyant torque is equal to the difference between the location of the CM and center of buoyancy (CB) along the x-axis multiplied by the buoyant force. The position of the CB relative to the stationary CM determines the directionality of the torque. If the CB is anterior to the CM, the body will rotate counterclockwise in lateral view, if it is posterior to the CM, the rotation will be clockwise. To find the CB of an individual disk, the immersed volume of the disk was multiplied by its centroid. The products were summed and divided by the volume of the immersed body as a whole to locate the model's CB.

Tests

Equilibrium—The models were at equilibrium when the buoyant and gravitational forces were equal and there was no rotation due to buoyant torque. The models approached equilibrium asymptotically. Due to the asymptotic nature, the model was cutoff once the difference between the gravitational force and buoyant force was less than 0.5% of the model's weight. The angle of inclination of the model at equilibrium was determined by measuring the angle formed by the waterline and a line running from the snout to the tip of the tail.

Buoyant Recovery—A buoyant recovery test determined how the models returned to equilibrium after submersion. The models were submerged in a horizontal orientation with full lungs and allowed to passively return to the surface. During buoyant recovery, the models were free to undergo translational adjustments and rotational adjustments about an axis perpendicular to the sagittal plane. The depth from which the models were released in the buoyant recovery tests differed by taxa and was dependant on body size. Release depth was determined by dividing the sum of the forces of gravity

and buoyancy by the weight of the model. The quotient was then multiplied by the maximum dorsoventral depth of the model.

Different release depths based on body size are necessary because of errors that arise due to inaccuracies in the body volume calculations being compounded when there is a strong positive buoyant force, as is the case when a model is rising to the surface. The errors are not noticeable if the models do not have to undergo much vertical displacement to reach equilibrium. If, however, it is released from a great depth, the calculation errors will result in a strong buoyant torque. The buoyant torque will cause counterclockwise rotation that orients the model in a vertical position with the tip of the snout pointing upwards. In this situation, the very tip of the snout will breach the water surface first and the model will fail to come to equilibrium once at the surface (Henderson, 2002). The release depths that are calculated for each model are just deep enough to show all of the stages of the recovery cycle, which reduces the impact of the inaccuracies of the volume calculations.

Lung Deflation—To test negative buoyancy via lung deflation, lungs with different volumes were added to the models. The lung volumes were decreased incrementally starting with 50% deflation and ended at the deflation needed for the model to sink. This negative buoyancy occurred when the force of buoyancy was decreased enough so that it was overcome by the force of gravity. In order to simulate deflated lungs, the dorsal margin of the lung cavity was kept constant and the ventral margin was moved dorsally until the desired lung volume was obtained.

Passive Recovery from Wave Action—In order to test stability at the water surface, the models were subjected to the effects of a wave hitting the lateral margin of

the animal causing a sideways tilt. To simulate this effect, the model were fully submerged with full lungs and given an initial tilt of nine degrees from the y-axis. The models were then allowed to return to equilibrium taking into account all of the forces and present in the previous tests with the addition of lateral rotation about the x-axis. The lateral rotation was determined by multiplying the distance between the CM and CB along the z-axis by the buoyant force. In anterior view, a CB located to the right of the CM resulted in a counterclockwise rotation and a CB to the left of the CM caused a clockwise rotation. To best show the lateral rotation during recovery, images of transverse cross sections through the trunk of the model were used to depict the recovery sequence, despite the fact that the test was applied to the model as a whole.

RESULTS

Models

With full lungs, the mean body densities of *Tatenectes*, *Cryptoclidus*, and *Thalassomedon* were 955 kg/m^3 , 931 kg/m^3 and 973 kg/m^3 respectively. While floating at equilibrium, the center of mass was dorsal to the center of buoyancy in all of the models, but the x-axis locations of the CM and CB were almost identical (less than three centimeters apart for all models). The location of the CM above the CB is the condition that is expected for objects floating at the surface. This is due to the fact that only the submerged portion of the object contributes to the location of the CB, whereas the CM is fixed and unaffected by the location of the object to the water surface. In *Tatenectes*, the CM is situated 0.170 m below the water surface and the CB is located 0.179 m below the surface. In *Cryptoclidus* the CM and CB are 0.167 m and 0.184 m below the surface

respectively. The CM and CB of the *Thalassomedon* model are at depths of 0.516 m and 0.543 m.

Tests

Equilibrium—At equilibrium, the entire dorsal surface of the head, neck, and back of the *Tatenectes* model rest above the surface of the water and the body has an angle of inclination of 5.28 degrees (Fig. 3.3a). The large portion of the model sitting above the water surface is probably not valid. There are several issues that the model does not take into account, which if applied, may cause the model to have more of its body submerged when at equilibrium. The model does not take into account the presences of the pachyostotic bones mentioned in Chapter 1, which may have affected the densities of the various body regions. In addition, the neck length and tail lengths of *Tatenectes* are unknown due to a lack of a preserved cervical and caudal vertebral series in the fossil record. It is possible that a longer neck would have shifted the CM of the model anteriorly and the model would have sat deeper, and more horizontal, in the water.

The *Cryptoclidus* model sits at an angle of 5 degrees to the water surface when at equilibrium (Fig. 3.3b). The anterior region from mid trunk is exposed at the surface, including the dorsal surface of the head. This equilibrium pose would have allowed for the animal to breath while at rest.

The angle of inclination in *Thalassomedon* is -1.34 degrees. The negative angle of inclination causes the head in *Thalassomedon* to be fully submerged (Fig. 3.3c), which would have hindered breathing. This equilibrium position may be a result of using a uniform density for the body. If the neck were less dense than the trunk and tail region, the CM would be moved posteriorly, possibly resulting in a model with the head breaking

the surface at equilibrium. Using the current uniform tissue densities, Dr. Henderson ran a model, which showed that *Thalassomedon* would have been capable of dorsal flexion of the neck to bring the head above the surface when necessary.

Buoyant Recovery—Using the equation described in the methods section, the depths of immersion for each model were determined. *Tatenectes* was released from a 0.65 m depth, *Cryptoclidus* from 0.5 m, and *Thalassomedon* was released from a depth of 1.5 m.

Tatenectes took the longest to recover equilibrium. It reached the water surface quickly; however, it took many minor adjustments once at the surface for the model to finally stabilize after 20 cycles. The adjustments at the surface were primarily rotation about the z-axis as the center of buoyancy shifted between being located anterior and posterior to the center of mass. *Cryptoclidus* and *Thalassomedon* recovered much quicker, both requiring only 8 cycles (Fig. 3.4). In *Tatenectes* and *Cryptoclidus*, there was a slight, positive buoyant torque that caused counterclockwise rotation of the sagittal plane, which lifted the head above the surface of the water. This resulted in the positive angles of inclination mentioned in the equilibrium section. In *Thalassomedon*, the buoyant torque resulted in a slight clockwise rotation, lifting the tail toward the water surface while dropping the head below the surface, therefore resulting in a negative inclination angle.

Lung Deflation—The lung capacity of the models was decreased in increments to find the percent lung deflation necessary for the models to become negatively buoyant. In *Tatenectes*, the lungs needed to be 90% deflated for the model to sink, *Cryptoclidus* required 95% lung deflation, and *Thalassomedon* became negatively buoyant at 85% lung deflation (Table 3.1). The mean densities of the models when they began to sink were

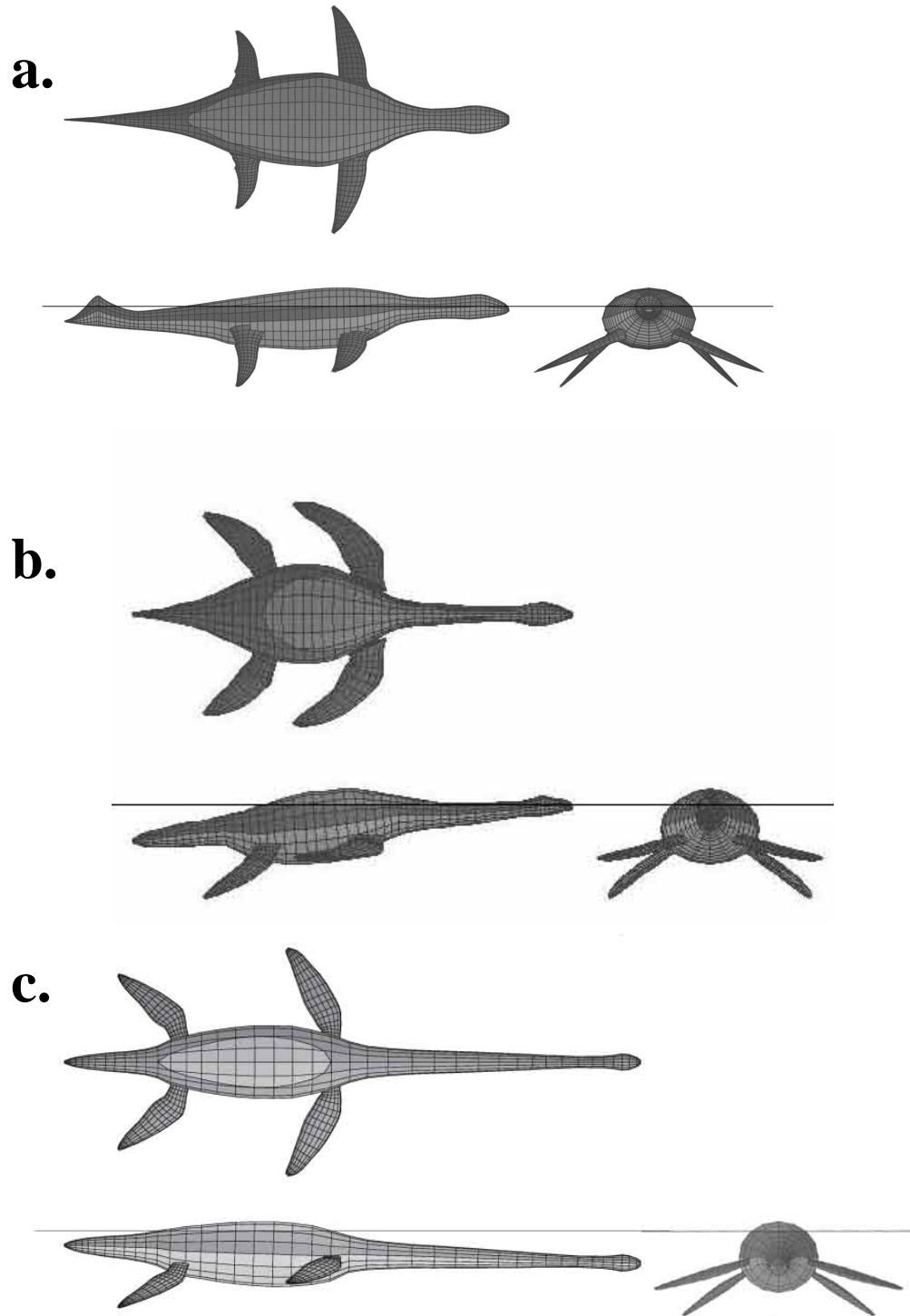


Figure 3.3. Models at equilibrium. The models in dorsal, lateral, and anterior views. The horizontal line represents the water surface and the dorsal regions with light shading are the regions above the water surface. **a.** *Tatenectes* **b.** *Cryptoclidus* **c.** *Thalassomedon*. (*Thalassomedon* figure is from Henderson, 2006).

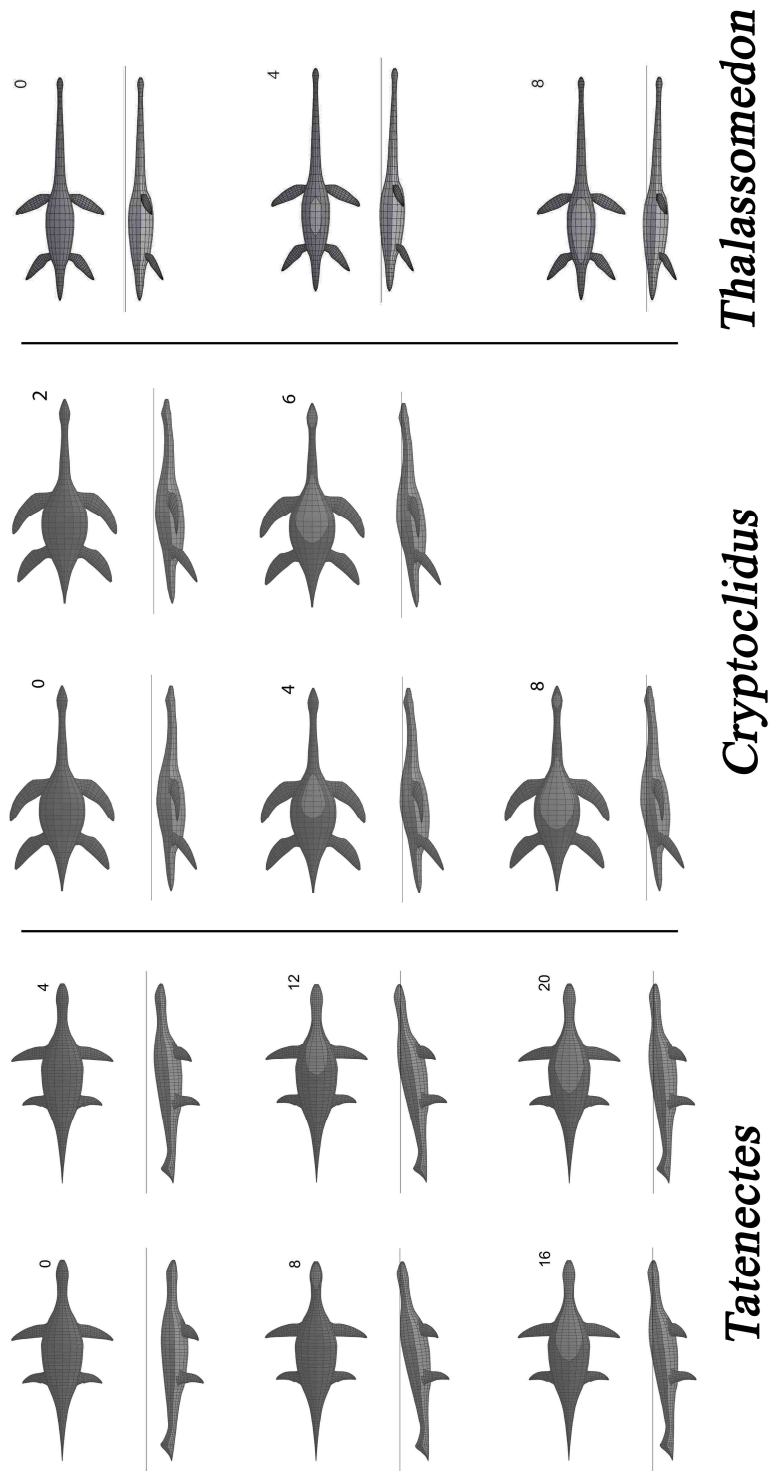


Figure 3.4. Buoyant recovery. Screen shots from the buoyant recovery of *Tatenectes*, *Cryptoclidus*, and *Thalassomedon*. The numbers in the upper right hand corners are the frame numbers of the screen shot. (*Thalassomedon* figure from Henderson, 2006).

very similar, ranging from 1038 kg/m³ in *Thalassomedon* to 1040 kg/m³ in *Tatenectes* (Table 3.1). The densities of the models when they become negatively buoyant are slightly higher than expected. In theory, the models should have started to sink when the density of the model exceeded the density of sea water (1026 kg/m³).

As with all of the models in Henderson’s 2006 paper, once the models began to sink the location of the CM and CB were almost identical (< 1 cm apart). This means that during negative buoyancy, the animals would not have experienced pivoting around the CM or lateral roll since both buoyant torque and rotation about the x-axis occur due to differences in the placement of the CM and CB along the x-axis and z-axis respectively. This suggests that differences in body shape would have had the most impact on passive stability while the animals were positively buoyant and at the water surface.

Table 3.1. The effects of lung deflation on body mean density and buoyancy.

Genus	Lung Deflation %	Mean Density (kg/m³)	Floating or Sinking
<i>Tatenectes</i>	50	1000	Floating
	80	1030	Floating
	85	1035	Floating
	90	1040	Sinking
<i>Cryptoclidus</i>	50	985	Floating
	80	1021	Floating
	85	1027	Floating
	90	1033	Floating
	95	1039	Sinking
<i>Thalassomedon</i>	50	1010	Floating
	75	1029	Floating
	80	1033	Floating
	85	1038	Sinking

Passive Recovery from Wave Action—The models that were dorsoventrally compressed in transverse cross section were the most stable. The dorsoventrally compressed *Tatenectes* recovered from the nine degree tilt in the fewest cycles, taking only 10 rotational cycles (fig. 3.5). *Cryptoclidus*, with its less compressed cross-sectional shape took 12 rotations to reach equilibrium (fig. 3.5). The deep body shape of the *Thalassomedon* was the least stable. It never actually reached perfect equilibrium, but was cut off after 25 cycles (fig. 3.5) as the final adjustments were very minor (Henderson, 2006).

DISCUSSION

Comparison

While floating at equilibrium, the short-necked *Tatenectes* and *Cryptoclidus* both had positive angles of inclination, while the long-necked *Thalassomedon* had a negative angle of inclination. These inclination angles resulted in head of the short-necked forms being elevated out of the water allowing for respiration while floating passively, whereas *Thalassomedon's* head was underwater and would have been required to flex its neck upward in order for the head to breach the water's surface.

After being released from depth and allowed to passively recover, both *Cryptoclidus* and *Thalassomedon* reached equilibrium quickly (in 8 cycles) compared to *Tatenectes* (20 cycles). The ability of *Cryptoclidus* and *Thalassomedon* to recover equilibrium in a few cycles suggests that the body shapes and positioning of the CM and CB are valid. The long recovery period of *Tatenectes* may be due to a miscalculation of the head and tail length, which could result in an erroneous CM and CB locations. This

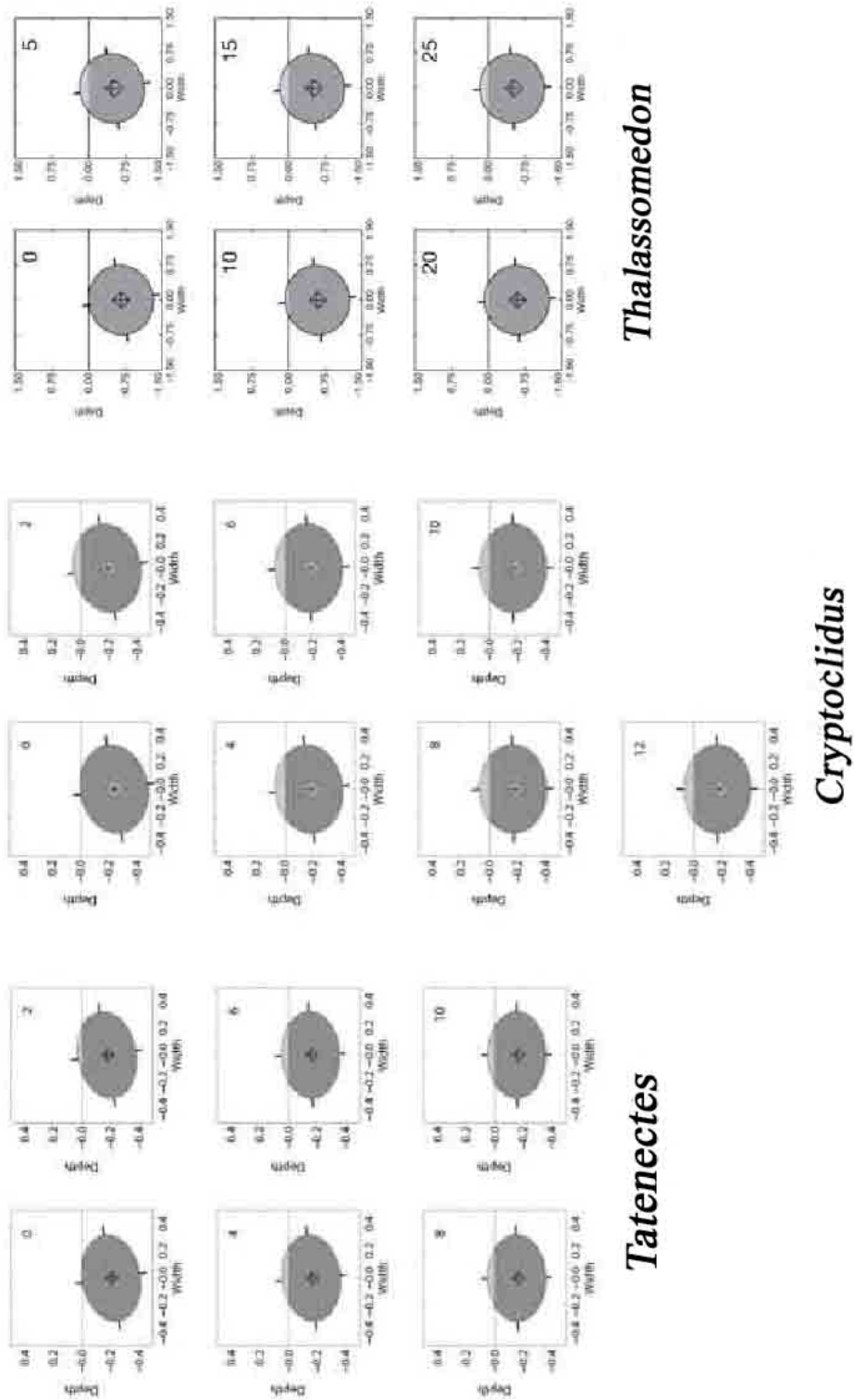


Figure 3.5. Lateral roll recovery. Screen shots from the recovery from a lateral roll of *Tatenectes*, *Cryptoclidus*, and *Thalassomedon*. The numbers in the upper right hand corners are the frame numbers of the screen shot, (*Thalassomedon* figure from Henderson, 2006).

CM and CB dislocation would have an effect on the buoyant torque, which is the dominant action once the model reaches the water surface. It is probable that a longer neck would have shifted the CM of the model anteriorly. This shift would not only modify the equilibrium pose of *Tatenectes*, but also change the buoyant recovery sequence. Once the correct neck length is determined, the model should experience less buoyant torque and therefore should recover in fewer than 20 cycles.

In all of the models, it was possible to achieve negative buoyancy by lung deflation alone. These findings lend support to the hypothesis of lung deflation as ballast. The mean density required to initiate sinking were slightly higher ($1038 \text{ kg/m}^3 - 1040 \text{ kg/m}^3$) than the than the expected density of 1026 kg/m^3 , which is the density of the seawater. This same slight discrepancy between the theoretical density needed for negative buoyancy and the observed density was noted by Henderson (2006). This difference is due to the fact that the volume calculations of each body slice are only an approximation. The computations of each body slice volume integral had to be cut off eventually in order for the tests to be run in a reasonable amount of time. As there are a large number of body slices, all of these rounding-off errors resulted in the computed sinking density differing from the theoretical sinking densities. However, this small variation (1.01%) from the ideal required density is not believed to significant.

Tatenectes and *Cryptoclidus* recovered in fewer cycles in the passive recovery from lateral roll test than *Thalassomedon*, requiring 10, 12, and 25 cycles respectively. The dorsoventrally compressed shape of *Tatenectes* made it the most stable, the position of the CB did not shift much due to the initial tilt and therefore did not require many adjustments before coming back in line with the CM. The slightly more round cross-

sectional shape of *Cryptoclidus* also provided stability. The deep bodied *Thalassomedon* was the least stable. The model continued to alternatively tilt left and right as the CB failed to ever come into perfect alignment with the CM along the y-axis.

Habitat Implications

A study done by Fish (2002) on maneuverability, habitat, and prey capture in cetaceans based on their cross-sectional shape found that deep bodied whales were less maneuverable than their flat bodied counterparts. The less maneuverable whales were found to be deeper water genera and feed on pelagic fish. The flat bodied, more maneuverable whales inhabit shallow water and coastal environments. They feed on bottom dwelling animals and zooplankton (Fish, 2002).

It is plausible that this same relationship between cross-sectional body shape and habitat existed within plesiosaurs. Based on Fish's research, the deep-bodied *Thalassomedon*, and likely *Muraenosaurus*, would have been deep water, pelagic foragers, whereas the dorsoventrally compressed *Tatenectes* and *Cryptoclidus* would have been slow-moving bottom feeders that inhabited shallow marine environments.

This relationship is also in accordance with the findings of the buoyancy and stability tests. Both *Tatenectes* and *Cryptoclidus* were able to recover quickly from wave action, which is a necessary trait for animals living in shallow water where they are more susceptible to waves than deep water animals. In deep water environments, the wave action is only prevalent at the surface, which would be an ideal environment for a less stable animal such as *Thalassomedon*. In addition, *Tatenectes* and *Cryptoclidus* were able to breathe while resting at the surface of the water, whereas *Thalassomedon* would not

have been comfortable able to do so and thus may not have spent much time at the surface.

Possible Sources of Error

There are several possible sources of error in the modeling method, which Henderson (2003) pointed out. One problem is that all of the models are of passive recovery of a static model. In reality, the animals would have been able to flex their bodies and move their appendages in order to actively stabilize themselves. Another factor is that the models do not take into account the effects of pressure changes. At depth, pressure changes would compress the lungs, increasing the density of the model. Changes in the density would have had the most effect on the buoyant recovery and sinking by lung deflation tests (Henderson, 2003). In addition to the sources of error within the modeling program, there are also some possible errors in the models themselves. The short neck of the *Tatenectes* model may not be correct. The exact impact that the neck and tail length have on the return of the model to equilibrium is uncertain.

Future Work

In future studies the tests for *Tatenectes* should be re-run using models with variable neck and tail length in order to determine the most plausible lengths. It would also be interesting to reconstruct the *Muraenosaurus* spinal column from a different specimen with a known vertebral order. The resulting reconstruction could then be used to create a computer model, which would allow researchers to determine the stability of an animal that is more deep bodied than *Thalassomedon*. The tests that were run in this study used the number of recovery cycles to determine the stability of the models. Future tests could be run that actually record the time that it takes for the models to reach

equilibrium as it could be argued that a more stable animal would be one that recovers equilibrium the fastest, if not necessarily in the fewest cycles. It would also be interesting to see if the same relationship between cross-sectional shape and recovery from wave action exists between cross-sectional shape and resistance to initiation of lateral roll while at the water surface. If so, it would lend additional support to the theory of dorsoventrally compressed plesiosaurs inhabiting shallow waters where the impact of wave action is more pronounced than in deep water environments.

CONCLUSION

Based on the anterior and posterior angle measurements taken while making the reconstructions of *Tatenectes*, *Cryptoclidus*, and *Muraenosaurus*, it is the rhomboidal shape of the vertebrae that is the cause of the curve. This differs from the spinal curvature in primates, which is caused by vertebral wedging. The height of the lateral spinal profiles played a large role in the cross-sectional shape of the animal. The flat profiles were associated with dorsoventrally compressed cross-sectional shape and high lateral profiles were associated with deeper body shapes. The data from the computer modeling tests suggest that flat bodied animals, such as *Tatenectes*, would have been more stable at the surface of the water than deep bodied animals such as *Thalassomedon*. If the correlation between body shape and environment seen in whales (Fish, 2002) is extended to plesiosaurs, the flat bodied *Tatenectes* and *Cryptoclidus* inhabited shallow marine environments and the deep bodied *Thalassomedon* inhabited pelagic environments.

Literature Cited

- Andrews, C. W. 1910. A Descriptive Catalogue of the Marine Reptiles of the Oxford Clay, Part I. British Museum (Natural History), London, England:1-205.
- Beaune, D., C. Le Bohec, F. Lucas, M. Gauthier-Clerc, Y. Le Maho. 2009. Stomach stones in king penguin chicks. *Polar Biology* 32:593-597.
- Brown, B. 1904. Stomach stones and food of plesiosaurs. *Science* 20(5):184-185.
- Brown, D. S. 1981. The English Upper Jurassic Plesiosauroidea (Reptilia) and a review of the phylogeny and classification of the Plesiosauria. *Bulletin of the British Museum (Natural History)* 35(4):253-347.
- Carpenter, K. 1996. A review of short-necked plesiosaurs from the Cretaceous of the Western Interior, North America. *Neues Jahrbuch für Geologie und Palaontologie* 201(2):259-287.
- Conybeare, W. D. 1824. On the discovery of an almost perfect skeleton of the *Plesiosaurus*. *Transactions of the Geological Society of London, Second Series* 1(2):381-389.
- Colbert, E. H. 1962. The weights of dinosaurs. *American Museum Novitates* 2076:1-16.
- Cruikshank, A. R. I., D. M. Martill, and L. F. Noe. 1996. A pliosaur (Reptilia, Sauropterygia) exhibiting pachyostosis from the Middle Jurassic of England. *Journal of the Geological Society, London* 153:873-879.
- Digiovanni, B. F., P. V. Scoles, B. M. Latimer. 1989. Anterior extension of the thoracic vertebral bodies in Scheuermann's kyphosis: An anatomic study. *Spine* 14(7):712-716.
- Druckenmiller, P. S. and A. P. Russell. 2008. A phylogeny of Plesiosauria (Sauropterygia) and its bearing on the systematic status of *Leptocleidus* Andrews, 1922. *Zootaxa* 1863:1-120.
- Fish, F.E. 2002. Balancing requirements for stability and maneuverability in cetaceans. *Integrative and Comparative Biology* 42:85-93.
- Gasparini, Z., N. Bardet, J. E. Martin, M. Fernandez. 2003. The elasmosaurid plesiosaur *Aristonectes* Cabrera from the latest Cretaceous of South America and Antarctica. *Journal of Vertebrate Paleontology* 23(1):104-115.
- Gregory, W. K. 1905. The weight of the brontosaurus. *Science* 22(566):572.

- Henderson, D. M. 1999. Estimating the masses and centers of mass of extinct animals by 3-D mathematical slicing. *Paleobiology* 25(1):88-106.
- Henderson, D. M. 2003. Effects of stomach stones on the buoyancy and equilibrium of a floating crocodylian: a computational analysis. *Canadian Journal of Zoology* 81:1346-1357.
- Henderson, D. M. 2006. Floating point: a computational study of buoyancy, equilibrium, and gastroliths in plesiosaurs. *Lethaia* 39(3):227-244.
- Ketchum, H. F. and R. B. J. Benson. 2010. Global interrelationships of Plesiosauria (Reptilia, Sauropterygia) and the pivotal role of taxon sampling in determining the outcome of phylogenetic analyses. *Biological Review* 85:361-392.
- Kriwet, J. and M. J. Benton. 2004. Neoselachian (Chondrichthyes, Elasmobranchii) diversity across the Cretaceous-Tertiary boundary. *Palaeogeography, Palaeoclimatology, Palaeoecology* 214:181-194.
- Lautrup, B. 2005. *Physics of continuous matter: exotic and everyday phenomena in the macroscopic world*. Institute of Physics Publishing.
- Lin, K. and O. Rieppel. 1998. Functional Morphology and Ontogeny of *Keichousaurus hui* (Reptilia, Sauropterygia). *Fieldiana: Geology N.S.*(39):1-35.
- Massare, J. A. 1988. Swimming capabilities of Mesozoic marine reptiles: implications for method of predation. *Paleobiology* 14(2):187-205.
- McHenry, C. R., A. G. Cook, S. Wroe. 2005. Bottom-feeding plesiosaurs. *Science* 310:75.
- Motani, R. 2001. Estimating body mass from silhouettes: testing the assumption of elliptical body cross-sections. *Paleobiology* 27(4):735-750.
- Motani, R. 2002. Swimming speed estimation of extinct marine reptiles: energetic approach revisited. *Paleobiology* 28(2):251-262.
- Novack-Gottshall, P. M. 2008. Using simple body-size metrics to estimate fossil body volume: empirical validation using diverse Paleozoic invertebrates. *Palaios* 23:163-173.
- Nowacek, D. P., M. P. Johnson, P. L. Tyack, K. A. Shorter, W. A. McLellan, D. A. Pabst. 2001. Buoyant balaenids: the ups and downs of buoyancy in right whales. *Proceedings of the Royal Society London* 268:1811-1816.
- O'Keefe, F. R. 2001. A cladistic analysis and taxonomic revision of the Plesiosauria (Reptilia: Sauropterygia). *Acta Zoologica Fennica* 214:1-63.

- O'Keefe, F. R. 2002. The evolution of plesiosaur and pliosaur morphotypes in the Plesiosauria (Reptilia: Sauropterygia). *Paleobiology* 28(1):101-112.
- O'Keefe, F. R. and M. T. Carrano. 2005. Correlated trends in the evolution of the plesiosaur locomotor system. *Paleobiology* 31(4):656-675.
- O'Keefe, F. R., H. Street. 2009. Osteology of the cryptocleidoid plesiosaur *Tatenectes laramiensis*, with comments on the taxonomic status of Cimoliasauridae. *Journal of Vertebrate Paleontology* 29(1):48-57.
- O'Keefe, F. R., H. Street, B. Wilhelm, C. Richards, and H. Zhu. 2011. A new skeleton of the cryptocleidid plesiosaur *Tatenectes laramiensis* reveals a novel body shape among plesiosaurs. *Journal of Vertebrate Paleontology* 31(2):330-339.
- Rasband, W. 2011. ImageJ version 1.44n. National Institutes of Health (available at <http://rsb.info.nih.gov/ij>).
- Smith, A. S. and G. J. Dyke. 2008. The skull of the giant predatory pliosaur *Rhomaleosaurus cramptoni*: implications for plesiosaur phylogenetics. *Naturwissenschaften* 95:975-980.
- Storrs, G. W. and M. A. Taylor. 1996. Cranial anatomy of a new plesiosaur genus from the lowermost Lias (Rhaetian/Hettangian) of Street, Somerset, England. *Journal of Vertebrate Paleontology* 16(3):403-420.
- Street, H. P. and F. R. O'Keefe. 2010. Evidence of pachyostosis in the cryptocleidoid plesiosaur *Tatenectes laramiensis* from the Sundance Formation of Wyoming. *Journal of Vertebrate Paleontology* 30(4):1279-1282.
- Tarlo, L. B. 1960. A review of Upper Jurassic pliosaurs. *Bulletin of the British Museum (Natural History)* 4(5):145-189.
- Taylor, M. A. 1981. Plesiosaurs—rigging and ballasting. *Nature* 290:628-629.
- Whitcome, K. K., L. J. Shapiro, D. E. Lieberman. 2007. Fetal load and the evolution of lumbar lordosis in bipedal hominins. *Nature* 450: 1075-1080.
- Wing, O. 2007. A review of gastrolith function with implications for fossil vertebrates and a revised classification. *Acta Palaeontologica Polonica* 52(1):1-16.